Assessment of Solar-Assisted Gas-Fired Heat Pump Systems

F. L. Lansing
DSN Engineering Section

Industrial and scientific communities are showing a new wave of interest in developing engine-driven heat pumps that utilize hybrid sources of energy combining fossil fuels, solar energy, and waste heat. As a possible application for the Goldstone Energy Project, the performance of a 10-ton heat-pump unit using a hybrid solar-gas energy source is evaluated in an effort to optimize the solar collector size. The heat-pump system is designed to provide all the cooling and/or heating requirements of a selected office building located at the Deep Space Communication Complex, Goldstone, California. The system performance is to be augmented in the heating mode by utilizing the waste heat from the power cycle. A simplified system analysis is described in this report to assess and compute interrelationships of the engine, heat pump, and solar and building performance parameters, and to optimize the solar concentrator/building area ratio for a minimum total system cost. In addition, four alternative heating-cooling systems, commonly used for building-comfort, are described; their costs are compared, and are found to be less competitive with the gas-solar heat-pump system at the projected solar equipment costs.

I. Introduction

Heat pumps, sometimes called "energy pumps," are mechanically driven devices that extract heat from one medium at a certain temperature and "pump" this heat and a little more to another medium at a higher temperature. If used for a heating purpose, heat pumps are known to have a high potential for saving natural energy resources and for reducing primary energy consumption as compared to direct electrical resistance heaters, or fossil-fuel-fired boilers. Several configurations exist, as illustrated in Appendix A, which differ mainly in the type of fluid or media exchanging heat with the heat pump's recirculating refrigerant.

The recent interest by industrial and scientific communities in energy-consumption reduction, as a result of the global energy-shortage situation, has stimulated more research and development of heat pumps in many areas, such as: (1) coupling with natural nonfossil-fuel energy resources such as solar-electric, biomass combustion or wind power, as prime movers, and (2) using the pump as a booster for any low-temperature heat, including waste heat, to obtain a more useful higher-temperature-level heat for industrial, residential, and commercial applications (Ref. 1).

Toward the commercialization of small-size heat-pump units (around 10 tons of refrigeration or 35.16 kWh_t) a new study is being jointly reviewed by the Energy and Technology Application office of the Jet Propulsion Laboratory (JPL) and Airesearch Manufacturing Company of the Garrett Corp., and is being sponsored and managed by the Department of

Energy. The hybrid heat-pump system concept under investigation replaces conventional electrical motor-drives with gas-fired engines (or turbines) coupled with solar concentrators. The solar connection is superimposed for saving additional gas heat during the sunny hours. Combining the expertise of JPL in high-temperature solar concentrators, solar receivers, high-temperature energy storage with and without phase-change materials (PCM), and building-energy analysis, with the experience of the Garrett Corp. in developing engines and gas-turbine hardware and in their computer simulation, the investigation is expected to be thorough and very informative.

As part of the Energy Conservation Project for the Deep Space Network (DSN) facilities, continually keeping aware of and making engineering assessments of new technologies, concepts, controls, components, and systems and their economics, particularly in the area of building heating, ventilation and air conditioning (HVAC), is of prime importance for upgrading the facilities and keeping their energy consumption at a minimum. The commercialization of the above hybrid heat-source system and its relevant advanced building controls presents an area worth investigating since it has a high potential for reducing the energy consumption of facilities and enhancing their energy self-sufficiency position.

Until the detailed computerized results of the above DOE-managed task are published, a short term definition study has been initiated in order to provide our facilities management and engineers with the key advantages of the candidate heat-pump configuration, its potential cost savings, and its performance and operational superiority. The task objectives are tentatively set to: (1) configure a complete add-on heat-pump system to an existing building at the DSN facility, (2) outline and identify by a simplified analytical approach, if possible, the key design and weather parameters, (3) compare its economics against alternate dual heating-cooling configurations that are commonly used, (4) provide an optimum solar-collector size for a minimum yearly total cost or a minimum 10-year life-cycle cost, and (5) study variances and sensitivities of the economics or configuration parameters including different types of buildings, weather patterns, energy rates, etc. This preliminary assessment is not intended to substitute for or replace the detailed work currently being done elsewhere, but rather to supplement it, and pave the way for examining to a first order of magnitude the concept applicability to existing DSN facilities that have different weather profiles, building loading, and building types.

The attractiveness of this solar-assisted gas-fired heat-pump system concept for future application in Deep Space Network buildings is based on several features, each of which offers potentially high efficiency, better utilization of existing fossil-fuel resources, or low cost. The system features are composed of the following elements:

(1) A heat pump that "pumps" heat, when used in the heating mode, from outdoor air. This is a single, compact device that functions as either a heating or a cooling unit as necessitated by the building needs.

(2) A heat recovery device that benefits from the heat rejected by the driving engine (or power cycle) and feeds a large portion of that heat directly to the conditioned space. This enables the system to out-perform conventional heating devices, which means higher performance, smaller solar collector area, and lower operation cost.

(3) No large thermal or electrical storage is required for this hybrid system since direct gas combustion is used when needed. Operation during the night or during cloudy periods is uninterrupted, thus providing high reliability.

The above features are expected to lead to savings in maintenance and operation costs.

Since numerous parameters are expected to enter into the system performance evaluation, two approaches could be followed: (1) a detailed computerized approach using hourly, daily, monthly, and yearly load distribution, component efficiency, and site weather, or (2) a simplified "lumping" approach for faster assessment. The first approach is already in progress with full results yet to be published. The second approach is the one chosen for this report in order to provide coarse boundaries, and size limits in the optimization of the solar share. The complexity of the second approach could be later increased for a better refinement of results accuracy by utilizing one of the available dynamic analysis computer programs such as TRNSYS, SOLTES, etc. However, this article reports only about the first-order assessment of the concept without any detailed computerized calculations.

II. System Description

An outline of a complete conceptual system driven by a hybrid solar/gas heat source is shown in Fig. 1. The flow of energy streams to and from each component is sketched in Fig. 2. The following 4 subsystems are identified:

(1) Solar collection and storage subsystem.

(2) Power conversion subsystem.

(3) Heat pump subsystem.

(4) Building air-handling subsystem.

The function of each subsystem is briefly described next, assisted by Figs. 1 and 2.

A. Solar Collection and Storage Subsystem

This subsystem consists of a solar concentrator, a solar receiver, and a high-temperature storage compartment. The concentrator is initially configured as a point-focusing 2-axis tracking paraboloid mirror. Appropriate mechanisms for adjusting the azimuth and elevation angles are provided to line up the paraboloid axis with the sun-earth vector during the sunny hours. The solar energy reflected by the concentrator mirror is focused on the finite aperture of the solar receiver, which is placed at the paraboloid focus. The solar receiver has a cavity-like shape to approximate a black-body radiator. It is also enclosed by a thermal insulation blanket to reduce the outward thermal radiation-convection losses to surrounding air. Through a set of heat-pipes connected to the interior solar receiver walls, a high-temperature energy-storage compartment is attached. The thermal storage capability of this subsystem may be limited to not more than one hour, to provide only damping and smoothing effects for the solar intensity fluctuations. Phase-change materials are recommended for a compact design and for their favorable small temperature changes during charging and discharging modes. The "useful" collected portion of the incident solar radiation, after subtracting the optical and thermal losses, represents heat available to be converted further to a mechanical energy form in the power conversion subsystem.

B. Power Conversion Subsystem

The hybrid heat source needed to operate this subsystem consists of: (1) high-temperature solar energy as delivered by the receiver-storage subsystem and (2) high-temperature products of combustion resulting from direct ignition, in a combustor, of a fossil fuel such as natural gas, propane, methane, etc.

The power conversion subsystem location is preferred to be next to the solar receiver-storage subsystem to minimize thermal losses. Gaseous or liquid fuels are also preferred for easy handling if transmitted in pipes to the focal region. For the present study, natural gas has been selected and is assumed available in the location under investigation.

In general, conversion of thermal energy to mechanical work is made via power cycles, of which the most important are:

(1) Brayton cycle, whether it is closed or open, simple or regenerative,

(2) Rankine cycle using water or organic fluids, and

(3) Stirling cycle

With any power cycle used, some heat must be rejected which, if recovered and utilized, represents a bonus to the overall system performance. The recoverable heat could be utilized directly for heating the building in the heating mode, and if needed, for temperature modulation in the cooling mode.

The system layout in Fig. 1 illustrates the components of one selected power cycle: The regenerative air-Brayton cycle, which is used as the prime mover for the heat pump. The power cycle is composed of an air compressor, an air turbine, a regenerator, a gas combustor and a heat sink. Air passes through the high-temperature energy-storage element to be heated before it enters the gas combustor. Gas combustion will take over as the sole heating source if insufficient solar energy is collected. The mechanical work of the power cycle is used to drive the refrigeration compressor by a single shaft as shown in Fig. 1. The solar receiver-storage subsystem and the power conversion subsystem could be placed in one assembly, located at the concentrator focal region. Combustion air is preheated before mixing with the fuel in the combustion chamber, by passing through the regenerator. The power conversion subsystem also includes the necessary air-flow controls to utilize the ambient air as a heat sink (if the heat rejected from the cycle is totally not needed) or else divert the air leaving the regenerator through air conduits to another heat exchanger (not shown in Fig. 1) connected to the building air-handler for additional heating, supplementing the heat-pump portion.

Note that configurations other than the selected Brayton cycle have been experimentally demonstrated by many researchers in this field. Steam turbines, for instance, are coupled with heat pumps for an integrated community energy system (Refs. 2, 3.). Other examples of using the organic Rankine turbo-compressor-driven heat pump include those of Mechanical Technology, Inc. (Ref. 4), the Institute of Gas Technology (Ref. 5), the United Technologies Research Center work using refrigerant R-11 (Ref. 6), the Battelle Columbus Laboratories work with R-11 as a power cycle fluid and R-12 as a refrigerant (Ref. 7), and the analysis of many working organic fluids for power cycles (Refs. 8 and 9). For a gas-fired free-piston Stirling engine driving a refrigeration compressor, experimental work was also demonstrated by the Gas Research Institute and General Electric Company for a 3-ton unit (Ref. 10). An internal combustion engine following the Otto-cycle, coupled with a heat recovery unit, a gas-fired auxiliary furnace, and a heat pump, was analyzed by Honeywell, Inc. for the Gas Research Institute (Ref. 11). A Stirling engine driving a unique Stirling refrigeration cycle was also demonstrated (Ref. 12).

C. Heat Pump Subsystem

A heat pump consists of the same basic components as a refrigeration machine, which are itemized as follows:

(1) An indoor element that adds heat to (in the heating mode) or extracts heat from (in the cooling mode) a medium in a conditioned space. This medium could be air or water.

(2) An outdoor element that extracts heat from or ejects heat to a medium outside a conditioned space. This medium also, could be air or water.

(3) A reciprocating or rotary compressor for compressing the refrigerant and moving it in the desired direction so that it "pumps" heat out or in, for cooling or heating modes.

(4) Control elements for satisfactory subsystem operation.

The functions of the refrigerant evaporator and condenser could be interchanged by reversing the direction of flow of the refrigerant between the indoor or outdoor elements. As illustrated in Fig. 3, in both cooling and heating modes, the major components are the refrigerant compressor, condenser, evaporator, throttling valve, and a mode-selector valve (i.e., a reversing valve). The mode-selector valve reverses the flow of refrigerant so that the indoor coil acts as an evaporator in the cooling mode and as a condenser in the heating mode.

The heat-pump subsystem could be any one of the four configurations described in Appendix A according to the medium type in contact with indoor and outdoor elements. The most common configuration, however, is the air-to-air (A-A) type. Performance data of A-A heat pumps appear in numerous references (e.g., Refs. 13 and 14), and in general the capacity and coefficient of performance are strong functions of outdoor temperature. As the temperature difference between indoor and outdoor air increases, it becomes more difficult to move the heat; thus, the capacities (for either heating or cooling) and the efficiency decrease.

Generally, a heat pump is designed to suit the peak cooling load. If the peak heating load exceeds the heating capacity of the pump, supplementary heat is commonly supplied by electrical resistance heaters. One should examine, however, the cost tradeoff of overdesigning the heat pump to cover the coldest winter load or using a suitably designed heat pump supplemented by another heating source. For multi-zone air conditioning systems using a heat pump, air changeover controls sometimes replace the refrigerant changeover valves, depending on the type of media exchanging heat with the pump. The refrigerant flow is not reversed in these systems.

The coefficient of performance, P, which is a measure of the heat-pump effectiveness, is defined as the ratio of "useful" heat effect delivered to the mechanical work used to operate the heat-pump subsystem:

$$P_c = \frac{Q_L}{W} \text{ (cooling mode)}$$

$$P_h = \frac{Q_H}{W} \text{ (heating mode)} \qquad (1)$$

Note that the P values should be based on the same operating conditions before making any comparison with other heat pump types. If compared to the ideal Carnot cycle behavior, the actual value of P is inversely proportional to the temperature difference between the heat source and heat sink. The larger this difference, the lower the performance will be. Because the P value varies with operating conditions, an average performance for the season seems more appropriate in comparing different systems in different climatic regions. In lieu of detailed thermodynamic evaluations (as given in Refs. 14 and 15) a simplified analysis is given in Appendix C based on graphs provided by Ref. 16.

D. Building Air-Handling Subsystem

As sketched in Fig. 1, the air movement to and from the conditioned space forms a closed loop. Fresh make-up air, which is the outdoor ventilation air, mixes with the return-air leaving the space, and the mixture is blown by a fan through the air-handler section. The air-handler is commonly composed of two coils, one for heating and the other for cooling, to adjust the air temperature to that required by the space according to its internal loads. Different temperature or flow controllers are used in practice for modulation. From an energy-balance viewpoint the air-handler requires a net heating or a net cooling effect which equals the heat lost or heat gained, respectively, from the gross control volume encompassing the space boundaries, air-handler, air ducts, and make-up air. In the heating mode, the heat-pump indoor element acts as a refrigerant condenser, i.e., as a heating coil, while use is made of a portion of the power cycle waste heat as a heating supplement. In the cooling mode, the heat-pump indoor element acts as a refrigerant evaporator, i.e., as a cooling coil. The power cycle waste-heat in this case could be entirely by-passed or partially used for temperature modulation. The physical location of the heat pump and the air-handler subsystem would probably be in a mechanical room in the building. Two fluid circuits connected to the focal assembly of the solar collection subsystem are envisioned. These are: (1) refrigerant lines connecting the refrigerant compressor to the heat-pump subsystem and (b) an air conduit connecting the power cycle

regenerator at the focal assembly with the air-handler "booster" coil.

The major system components having been described, a set of analytical expressions will be presented next to describe the system operation and design guidelines.

III. System Analysis

The following assumptions and idealizations are made in the analysis of the system in order to yield a simplified approach and to enable a complete assessment without a great loss of accuracy.

(1) The exterior outside air temperature variations throughout the year are divided into only two seasons: summer and winter. Spring and fall periods will be merged as appropriate. Distinction between summer and winter is assumed to take place when the average daily temperature, t_o, exceeds or is below a reference temperature. On the other hand, the cooling and heating modes of system operation occur for M_c and M_h months, respectively, which are not necessarily equal but total 12. Modes of operation are determined by comparing the daily average outside air temperature with the building changeover temperature, T_o*. There is always a possible overlap between seasons and modes of operation depending on the type of air-handler modulation, local weather profiles, and space internal loads. The daily average outside air temperature $t_{o,c}$ or $t_{o,h}$ for either cooling or heating modes, respectively, are obtained from local weather data. The building changeover temperatures (one for each season is assumed) are obtained from space internal loads, interior temperature, and rate of heat loss to ambient.

(2) The efficiency of the concentrator mirror, if defined by the ratio of solar flux on receiver interior walls to the solar flux falling on mirror projected areas, becomes the product $\rho\phi$ where ρ is the mirror reflectivity and ϕ is the intercept factor. The intercept factor is defined as the fraction of the reflected radiation from the concave mirror that is intercepted by the internal cavity surface of the solar receiver. The intercept factor is a property of both the concentrator mirror's orientation for producing an image and the receiver's position relative to the concentrator. The optimum aperture size with a mirror of given optical properties, is commonly made by maximizing the "useful" energy collected by the mirror-receiver or minimizing the sum of their optical and thermal losses. A large receiver aperture results in large thermal losses but small optical losses, and vice versa.

(3) Cavity solar receivers are generally high-efficiency absorbers. The receiver, when coupled with the adjacent high-temperature energy storage element, has an efficiency that is defined as the ratio of useful collected thermal energy (which crosses the receiver-storage boundary to the power conversion subsystem) to that energy incident upon the receiver interior walls. Writing the energy collection subsystem efficiency R approximately as a linear relationship with the temperature difference between the receiver working fluid and the ambient air, yields:

$$R = F\rho\phi\alpha - FU\left(\frac{T_f - T_o}{I}\right) \qquad (2)$$

where T_f is the inlet fluid temperature to the receiver, ρ is the mirror reflectivity, α is the effective receiver absorptivity, F is a flow factor, I is the solar intensity, and U is the overall heat-loss rate due to convection and radiation per unit concentrator area. Note that the coefficient U takes into consideration the concentration ratio, receiver geometry, etc. Equation (2) could be also written in the linear form:

$$R = m_s - n_s\left(\frac{T_f - T_o}{I}\right) \qquad (3)$$

where the intercept m_s represents the product $(F\rho\phi\alpha)$ and the slope n_s represents the product (FU).

Solar concentrators with a concentration ratio between 100 and 1000 could reach fluid temperatures between 500°C (932°F) and 1000°C (1832°F). The intercept m_s, for high-temperature solar concentrators, ranges from 0.8 to 0.9, and the slope n_s ranges from 0.10 to 0.20 W/m²°C.

(4) The efficiency of a general power conversion subsystem is here simplified by a fraction λ_e of the corresponding Carnot's cycle operating between the temperature limits T_f and T_o. By this method, the distinction between different types of power cycles is made primarily by knowing the fraction λ_e, which is commonly limited to a value between 0.4 and 0.6 in practice; thus

$$E = \lambda_e\left(1 - \frac{T_o}{T_f}\right) \qquad (4)$$

(5) Similar to the power conversion subsystem performance, the coefficient of performance of a general heat pump P, in either cooling or heating modes at

full load, could be approximated as a constant fraction λ of the Carnot's ideal refrigeration cycle operating between the same evaporator and condenser temperatures, T_{ev} and T_{co}. Hence,

$$P_h = \lambda_h \left(\frac{T_{co}}{T_{co} - T_{ev}} \right)_h \tag{5}$$

$$P_c = \lambda_c \left(\frac{T_{ev}}{T_{co} - T_{ev}} \right)_c \tag{6}$$

For a given space inside temperature, T_i, and a given outside air temperature, T_o, the performance of an air-air heat pump for instance could be evaluated by determining the temperature drop across the evaporator Δt_{ev} and across the condenser Δt_{co} as presented in Appendix C. Note that the fractions λ_h, λ_c embody other design factors such as the type of medium used (water or air), partial loading, and all temperature, pressure, and flow control schemes. In the heating mode, the coefficient of performance P_h as given by Eq. (5) decreases as the outside air temperature (or condenser temperature T_{co}) decreases, thus reducing the amount of heat "pumped" to space. For the cooling mode, Eq. (6) gives a lower P_c as the outside air temperature increases, thus reducing the cooling effect of the refrigerator. This means that in both modes, the trend of the heat pump performance is always against the response of building loads at different outside temperatures. This supply and demand contrast could be illustrated by Figs. 4 and 5, which will be further explained in the analysis later on.

(6) The internal heat gain to (or loss from) a building space, is given in detail in Ref. 17 and is sketched in Fig. 4. The load is assumed the sum of the following four parts:

First, the internal heat generated due to occupant-activity, lighting equipment, electronic equipment, mechanical equipment with motor drives, and internal fuel-fired appliances. This is treated as a constant load independent of outside air temperature variations, but subject to variations in the schedule of activities inside the space.

Second, the heat transmitted to the building structure directly due to solar-radiation incidence upon glazing areas and indirectly due to solar-radiation incidence on opaque exterior walls and roofs. This part is also assumed a constant load, independent of the outside air temperature variations although it takes into consideration reradiation to the sky.

Third, the heat transmission due to varying outside air boundary-layer temperature next to exterior walls, roofs, and windows. If averaged over 24 hours, transient effects are damped and this part is found to be proportional to the difference between the daily average inside and outside air temperatures.

The fourth part of the space load is the undesirable heat loss (or gain) due to infiltration and ventilation. Infiltration or exfiltration air is caused by leakages through cracks or repeated opening of doors, and windows, or due to buoyancy effects. Ventilation air, on the other hand, is essential for hygienic purposes. Since the introduction of outdoor air, whether it is desirable or not, is an energy extensive process, the amount of such air should always be kept at a minimum rate. The sensible heat load as a result of this fourth part will be proportional to the difference between inside and outside air temperatures.

By neglecting latent loads in comparison with sensible loads, and by taking the minimum period of analysis as one day (24 hours), heat gain to a space per unit floor area Q_b could be written simply by the straight line relation.

$$Q_b = m_b + n_b (T_o - T_i) \tag{7}$$

where m_b is a constant building load intercept combining the first and second constant parts of heat gain, n_b is a building load slope combining the third and fourth parts of the heat gain, T_i and T_o are the daily average inside and outside dry bulb temperatures, respectively. The monthly calculations of Q_b are made for one selected day for each month. Monthly space loads could be assumed repeated images of this single representative day in each month. Although daily or monthly values for the parameters m_b and n_b could be used, only two possible patterns for m_b and n_b are allowed for the yearly building load computation, one for the summer and the other for the winter season. Numerically, the values of m_b and n_b are subject to simple design criteria that are usually given per unit floor area (Ref. 17). Furthermore, variations of m_b and n_b are known to be mainly dependent on the type of building activity (e.g., an office building, a central control building, a cafeteria, etc.) and to a lesser extent on the local climate.

Of special importance to the building mode of operation is a particular outside air temperature at which the gross building load reaches zero. This is sometimes called the changeover temperature, T_o^*, which is given by equating Eq. (7) to zero; hence

$$T_o^* = T_i - \frac{m_b}{n_b} \tag{8}$$

The characteristic temperature T_o^* represents the outside air-building "equilibrium" temperature where a lower outside air temperature (i.e., $T_o < T_o^*$) means the building is in a heating mode, and a higher outside air temperature (i.e., $T_o > T_o^*$) means the building is in a cooling mode. Differentiation between a heating mode and a cooling mode is therefore a necessary step once the temperature T_o^* is determined, and should be distinguished from summer and winter seasons.[1]

(7) For a given heat-pump cooling capacity, or heat-pump rating, CC (taken at the ARI temperature specification of 35°C (95°F)), the design space floor area to match this capacity is determined based on the peak cooling demand of the space. Let the heat-pump cooling capacity change with the outside air temperature (Ref. 16) as

$$CC_{to} = CC_{35}\,[1 - 0.018\,(t_o - 35)] \tag{9}$$

where CC_{to} is the cooling capacity in tons of refrigeration[2] at any outside air temperature, CC_{35} is the rated capacity at 35°C (95°F), and t_o is in °C. Figure 6 illustrates the difference between the building heat gain and the heat-pump cooling output[3] at various outside air temperatures. At the summer design outside air temperature of the site, $\bar{t}_{o,c}$, the pump's cooling capacity (point A in Fig. 6) should be somewhat larger than the building's peak heat gain (point B in Fig. 6) by a 10-20% margin to allow for extreme weather conditions. By taking an arbitrary 15% capacity margin, the appropriate space area that could be handled by a given heat pump capacity is calculated from Eqs. (7) and (9) as:

$$A_b = \frac{3057\,CC_{35}\,[1 - 0.018\,(\bar{t}_{o,c} - 35)]}{m_{b,c} + n_{b,c}\,(\bar{t}_{o,c} - t_{i,c})} \tag{10}$$

where the coefficients $m_{b,c}$ and $n_{b,c}$ are expressed in SI units in W/m² and W/m²°C, respectively, CC_{35} in tons of refrigeration and A_b in m². Eq. (10) could be also used if the building floor area is given and the appropriate cooling capacity needs to be known.

(8) The annual cost of purchased gas energy at a particular mode of operation is determined by the part of the building load which is unmet by solar energy assistance, taking into consideration the efficiencies of the various components. During M_h months of the heating period, the total cost of gas energy C_h becomes the sum:

$$C_h = C_g \sum_{M_h} \left[\frac{730 A_b \cdot |Q_{b,h}|}{COP_{g,h}} - \frac{30.42\,A_s S_h\,COP_{s,h}}{COP_{g,h}} \right] \tag{11}$$

where C_g is the unit gas energy cost in \$/W, $COP_{g,h}$ and $COP_{s,h}$ are the gross coefficients of performance of the system in the heating mode, driven by either gas combustion or solar radiation, respectively, and S_h is the effective daily solar radiation incident upon the concentrator projected area A_s. Eq. (11) assumes a standard month of 30.42 days and 730 continued working hours. The gross coefficient of performance in the heating mode COP_h is determined from Fig. 7, where two types of energy sources are identified: the first being solar radiation and the second gas combustion. COP_h is defined as the ratio of the cumulative heating effect to the space divided by the input primary energy source. From Fig. 7, $COP_{s,h}$ and $COP_{g,h}$ are written as:

$$COP_{s,h} = [\eta_w + E_{s,h}\,(P_h\,\eta_t - \eta_w)]\,R_h \tag{12}$$

$$COP_{g,h} = [\eta_w + E_{g,h}\,(P_h\,\eta_t - \eta_w)]\,\eta_g \tag{13}$$

Similarly, during M_c months of the cooling period, the total yearly cost of gas energy becomes

$$C_c = c_g \sum_{M_c} \left(\frac{730\,A_b \cdot Q_{b,c}}{COP_{g,c}} - \frac{30.42\,A_s S_c\,COP_{s,c}}{COP_{g,c}} \right) \tag{14}$$

where $COP_{g,c}$ and $COP_{s,c}$ are the gross coefficients of performance of the system in the cooling mode, driven by either gas combustion or solar radiation,

[1] Most weather stations make the distinction of a heating-degree-day and a cooling-degree-day based on the difference between the daily average outside air temperature and 18.33°C (65°F) as a reference temperature.

[2] One ton of refrigeration equals 12,000 Btu/hr or 3516 W.

[3] The cooling capacity and heating capacity of a heat pump are approximately equal to each other at rated conditions. The pump is usually designed to satisfy the peak building cooling needs, and if it is not able to satisfy the peak heating needs, a supplement heater is used. Otherwise, the pump is slightly overdesigned to satisfy both needs completely.

respectively, and S_c is the effective daily solar radiation incident upon the concentrator projected area. Fig. 8, as in Fig. 7, illustrates quantitatively the energy flows for the cooling period where the gross coefficients $COP_{g,c}$ and $COP_{s,c}$ are given by:

$$COP_{s,c} = R_c E_{s,c} \eta_t P_c \tag{15}$$

$$COP_{g,c} = \eta_g E_{g,c} \eta_t P_c \tag{16}$$

By using Appendix B, several expressions for the maximum $COP_{s,h}$ and $COP_{s,c}$ could be derived to obtain the optimum receiver-engine working temperature. The energy calculations are made monthly and then summed to obtain the yearly profile.

(9) The yearly cost of gas heating, given by Eq. (11), could be further written as:

$$C_h = A_b \sum_{M_h} \left(\beta_{b,h} - \beta_{s,h} \frac{A_s}{A_b} \right) \tag{17}$$

where the monthly cost parameters $\beta_{b,h}$ and $\beta_{s,h}$ are given by:

$$\beta_{b,h} = 730\, C_g\, |Q_{b,h}| / COP_{g,h} \tag{18}$$

$$\beta_{s,h} = 30.42\, C_g S_h\, COP_{s,h} / COP_{g,h} \tag{19}$$

The parameter $\beta_{b,h}$ at a particular month represents the gas heating energy cost per unit building area if no solar equipment exists, where heating is exclusively provided by the gas-fired heat pump. However, the parameter $\beta_{s,h}$ represents the gas cost savings, per unit collector area, resulting from adding a solar collector. The cost C_h starts with a value of $\beta_{b,h} A_b$ if no solar collector is connected and drops nonlinearly to zero cost at the maximum collector area $\bar{A}_{s,h}$, where the cost C_h remains zero thereafter. The area $(\bar{A}_{s,h}/A_b)$ given by $(\beta_{b,h}/\beta_{s,h})$ for the month of peak load represents the maximum collector area required to satisfy the building's peak heating load. Note that by subtracting the terms $\beta_{b,h} A_b$ and $\beta_{s,h} A_s$ for any month during the heating mode, negative values of C_h (when $\beta_{b,h} A_b < \beta_{s,h} A_s$) must be counted as zero, which makes the C_h curve with the area A_s a nonlinear relationship, as shown in Fig. 9.

(10) The yearly cost of gas energy for cooling, given by Eq. (14), could also be rewritten similarly to Eq. (17) as:

$$C_c = A_b \sum_{M_c} \left(\beta_{b,c} - \beta_{s,c} \frac{A_s}{A_b} \right) \tag{20}$$

where the monthly parameters $\beta_{b,c}$ and $\beta_{s,c}$ are given by:

$$\beta_{b,c} = 730\, C_g\, Q_{b,c} / COP_{g,c} \tag{21}$$

$$\beta_{s,c} = 30.42\, C_g S_c\, COP_{s,c} / COP_{g,c} \tag{22}$$

By analogy, the parameter $\beta_{b,c}$ represents the monthly gas energy cost per unit building area when cooling is exclusively provided by the gas-fired heat pump, without solar equipment. Also, the parameter $\beta_{s,c}$ represents the monthly cost savings, per unit collector area, resulting from adding a solar collector. The yearly cost of gas-cooling is initially $\beta_{b,c} A_b$ with no solar equipment and drops nonlinearly as the concentrator area increases to a collector area $\bar{A}_{s,c}$, where the cost remains zero thereafter. The area ratio $\bar{A}_{s,c}/A_b$ as calculated from $(\beta_{b,c}/\beta_{s,c})$ at the peak cooling month, represents the maximum collector area required to satisfy the building's peak cooling load. Analogously to the heating mode, by subtracting the monthly values of $\beta_{b,c} A_b$ from $\beta_{s,c} A_s$ some differences may result in negative values (when $\beta_{s,c} A_s > \beta_{b,c} A_b$), which should be counted as zero. This again gives a convex-shape curve for C_c vs A_s as sketched in Fig. 9.

(11) To compare the economics of candidate heating/cooling systems, several life cycle cost methodologies are available in the literature. One such method is to compute the accumulated implementation, maintenance, and operation costs over a certain number of years, N (e.g., 10 years, 15 years, or the life time of the major system components). Consideration could be taken of some or all of several economic factors such as general inflation rate, taxes, insurance, money interest rates, escalation of maintenance costs, escalation of energy costs, etc. A second method in economic comparisons is to divide the N-year life cycle cost into a "levelized" total cost, LTC, for each year of system operation. By adopting this method, the total annual cost of the gas-fired heat pump system with and without solar equipment is given by:

$$LTC = C_h + C_c + C_m + C_{im} \times CRF \tag{23}$$

where C_h and C_c are the annual costs of energy consumed for heating and cooling, respectively, C_m is the annual maintenance cost, C_{im} is the implementation cost of the new or add-on system including the

hardware and installation costs, and *CRF* is the cost recovery factor. The *CRF*, defined as the annual payment of 1$ borrowed with *i*% interest rate, and *N* years payment period, is obtained from:

$$CRF = i(1+i)^N/[(1+i)^N - 1] \qquad (24)$$

To compare the economics of the solar-assisted gas-fired heat pump under study with another gas-fired pump without solar equipment, the costs C_h and C_c, are obtained from Eqs. (17) and (20), respectively. As sketched in Fig. 9, the yearly gas cost for heating, C_h, starts with $A_b \sum_{M_h} \beta_{b,h}$ if no solar concentrator is present and decreases in a nonlinear relationship as the concentrator area A_s increases until a zero cost is reached when all heating loads are provided by the solar energy. Similar nonlinear behavior is shown for the yearly gas cost for cooling, C_c, when the monthly load profile is actually computed. If the monthly building loads during a particular mode of operation, however, is averaged as shown by profile 2, Fig. 9, the relationships between C_h or C_c and A_s become linear but lead to a gross error in computing the optimum collector area, as analyzed later on.

To account for the costs of financing, property taxes, insurance, maintenance, etc., one can simply multiply the system implementation cost by an Annual Cost Factor, *ACF* (Ref. 18), thus giving a slightly different value to *CRF* as given by Eq. (24). Either an effective *CRF* or *ACF* will be used to combine the yearly costs of implementation and maintenance.

(12) A general profile of the levelized total cost, *LTC*, versus the concentrator area A_s (or the ratio A_s/A_b) is sketched in Fig. 10 for an add-on solar equipment option. The total gas energy cost ($C_c + C_h$), the solar-equipment implementation and maintenance costs [$C_m + C_{im} \times CRF$], are sketched as shown in Fig. 10. The energy cost decreases as the concentrator area increases but, on the other hand, the implementation cost increases. Hence, the levelized total cost, *LTC*, reaches a minimum at the optimum concentrator size A_s^*. On the other hand, A_s^* could be given by differentiating Eq. (23) with respect to A_s (assuming C_m, *CRF* as constants), and equating to zero.

$$C_s \times CRF = \frac{-d}{dA_s}(C_c + C_h) \qquad (25)$$

where C_s ($/m^2) is the differential concentrator cost per unit area. The optimum concentrator size could be obtained either graphically or by the next analytical method. If the costs C_c and C_h are fitted, each, approximately by a quadratic relation in A_s:

$$\left.\begin{aligned} C_c/A_b &= a_{1,c} + a_{2,c}\left(\frac{A_s}{A_b}\right) + a_{3,c}\left(\frac{A_s}{A_b}\right)^2 \\ C_h/A_b &= a_{1,h} + a_{2,h}\left(\frac{A_s}{A_b}\right) + a_{3,h}\left(\frac{A_s}{A_b}\right)^2 \end{aligned}\right\} \qquad (26)$$

Hence, the coefficients a_1, a_2 and a_3 should be known from 3 key properties of the annual energy cost profile. The first coefficient, a_1, for both heating and cooling modes, could be determined by using Eqs. (17) and (20) and Fig. 9 when the concentrator area A_s is set equal to zero:

$$\left.\begin{aligned} a_{1,h} &= \sum_{M_h} \beta_{b,h} \\ a_{1,c} &= \sum_{M_c} \beta_{b,c} \end{aligned}\right\} \qquad (27)$$

The second coefficient, a_2, in both heating and cooling modes, represents the initial slope at $A_s = 0$; therefore, at very small A_s close to zero, one may write from Eqs. (17) and (20):

$$\begin{aligned} a_{2,h} &= -\sum_{M_h} \beta_{s,h} \\ a_{2,c} &= -\sum_{M_c} \beta_{s,c} \end{aligned} \qquad (28)$$

Accordingly, the coefficients a_1 and a_2 will represent the gas cost coefficients if the space load is approximated as a constant, uniformly distributed load over a particular mode of operation. Since the actual space load varies on a daily or a monthly basis and is not constant over all the year, the third coefficient, a_3, will represent the side effect of actual load deviations from those average conditions. In fact, the coefficient a_3 of Eq. (26) is the sole driver behind the nonlinear relationship previously described. Finally, in order to fit Eq. (26) to the peak load condition where a large solar concentrator area is built to entirely cover the load needs, the coefficient a_3 is found from:

$$\left.\begin{aligned} a_{3,h} &= \frac{-a_{1,h}}{(\bar{A}_{s,h}/A_b)^2} - \frac{a_{2,h}}{(\bar{A}_{s,h}/A_b)} \\ a_{3,c} &= \frac{-a_{1,c}}{(\bar{A}_{s,c}/A_b)^2} - \frac{a_{2,c}}{(\bar{A}_{s,c}/A_b)} \end{aligned}\right\} \quad (29)$$

where $\bar{A}_{s,h}$ and $\bar{A}_{s,c}$ are the concentrator areas that satisfy peak heating and peak cooling loads, respectively. Upon the determination of the fitted coefficients a_1, a_2, and a_3 from Eqs. (27) - (29), coupling of Eqs. (25) and (26) yields the optimum concentrator area A_s^* as:

$$\frac{A_s^*}{A_b} = \frac{\sum_{M_h} \beta_{s,h} + \sum_{M_c} \beta_{s,c} - C_s \times CRF}{2\left[\dfrac{\sum_{M_h} \beta_{s,h}}{(\bar{A}_{s,h}/A_b)} - \dfrac{\sum_{M_h} \beta_{b,h}}{(\bar{A}_{s,h}/A_b)^2} + \dfrac{\sum_{M_c} \beta_{s,c}}{(\bar{A}_{s,c}/A_b)} - \dfrac{\sum_{M_c} \beta_{b,c}}{(\bar{A}_{s,c}/A_b)^2}\right]} \quad (30)$$

Eqs. (25) and (30) and Fig. 10 suggest that the solar concentrator designer should build an ever increasing concentrator size until the "marginal cost" (or the slope of cost curve) of added-on solar equipment (which is in turn the marginal cost of gas energy displaced by solar) equals the "marginal cost" of saving gas energy, i.e., when the slope of the two energy saving and implementation curves becomes the same.

Equation (30) is an important expression needed to find the optimum collector area A_s^*. While it includes the key parameters of the system, Eq. (30) is only valid in the range $(A_s/A_b) = 0$ up to the limiting (A_s/A_b) for either heating or cooling, whichever is smaller. Note that the form of Eq. (30) could be further written in terms of the space cooling/space heating load ratio, for different types of buildings or for different weather patterns. However, this was not done because of its complex form.

(13) For the solar-assisted system to have economic feasibility, two conditions should be met in general. These are explained as follows:

(a) Non-negative concentrator area condition ($A_s^* \geq 0$). This constrains the concentrator area cost, C_s, to be always below a maximum value. Since the denominator of Eq. (30) is always positive, then:

$$(C_s)_{\max} = \left(\sum_{M_h} \beta_{s,h} + \sum_{M_c} \beta_{s,c}\right)/CRF \quad (31)$$

(b) Ceiling *LTC* condition: The levelized total cost of the solar-assisted system must not be more than the *LTC* of the original system without solar equipment. This means that after the determination of the optimum ratio $(A_s/A_b)^*$, the resulting minimum *LTC* must satisfy the following condition:

$$LTC^* < A_b\left(\sum_{M_h} \beta_{b,h} + \sum_{M_c} \beta_{b,c}\right) \quad (32)$$

The above assumptions, idealizations, and economic feasibility conditions are illustrated for a sample office-type building at a selected DSN facility.

IV. System Application

An office building at the Deep Space Network Communication complex, Goldstone, California has been selected for the numerical evaluation of the system design and optimization. The detailed itemization of the building loads in both the summer and winter seasons appears in Ref. 17, for an arbitrarily selected floor area. However, the unit area parameters m_b and n_b were assumed independently of the building area to enable computations of the matching space size using Eq. (10) for a given heat-pump capacity. Other information is categorized as follows:

Weather		
Outside air design temperature,[4] $\bar{t}_o$		
	summer	37.78°C (100°F)
	winter	-2.22°C (28°F)
Months of season[4]		
	summer	5 ($t_o > 18.33$°C)
	winter	7 ($t_o < 18.33$°C)
Seasonal average outside air temperature		
	summer	25.8°C (78.46°F)
	winter	11°C (51.84°F)

[4] See Table 1 for monthly outdoor temperature and solar radiation profiles, taken from Refs. (19) and (20).

Effective daily solar input[5]	
summer	7548 Wh/m^2 day
winter	6616 Wh/m^2 day
Seasonal average solar intensity, I	
summer	943 W/m^2
winter	880 W/m^2

Building Specifications

Constant load per unit area,[6] m_b	
in summer	37.0 W/m^2
in winter	31.7 W/m^2
Rate of heat loss to or gain from ambient[7], n_b	4.783 W/m^2°C (0.84 Btu/h ft^2°F)
Indoor design temperature[8], T_i	
in summer	25.56°C (78°F)
in winter	22.22°C (72°F)
Changeover Temperature[9], T_o^*	
in summer	17.82°C (64.1°F)
in winter	15.59°C (60.1°F)
Matching Building Area,[10] A_b	304 m^2 (3275 ft^2)

Concentrator-Receiver

Mirror reflectivity, ρ	0.88
Aperture intercept factor, ϕ	0.97
Receiver flow factor, F	0.94
Receiver effective absorptivity, α	0.90
Thermal loss rate, U	0.17 W/m^2°C
Collector efficiency intercept,[11] m_s	0.722
Collector efficiency slope,[11] n_s	0.160 W/m^2°C

[5] Allows for 20% of the incident solar energy from Table 1 to be ineffective for tracking during sunrise and sunset hours.

[6] Includes lighting, mechanical equipment, electronics equipment, and solar heat gain to space directly through fenestration areas and indirectly through opaque walls, from Ref. (17).

[7] Includes heat transmission to and from varying ambient temperatures, ventilation, infiltration and exfiltration air effects. This is assumed the same for both summer and winter seasons (Ref. 17).

[8] Follows ASHRAE 90-75 standards (Ref. 13).

[9] T_o^* corresponds to a zero building load Q_b from Eq. (8).

[10] Using Eq. (10) with a 10-ton heat-pump cooling capacity, and a margin capacity of 15% over peak building cooling load when both building and pump are at an outdoor air design temperature, $\overline{t_o}$, of 37.78°C (100°F)

[11] From Eq. (3).

Fluid operating temperature,[12] t_f,	
heating mode	500°C (932°F)
cooling mode	800°C (1472°F)

Power Conversion Subsystem

Efficiency of power transmission to the heat pump compressor,[13] η_t	0.9
Gas combustor efficiency, η_g	0.85
Ratio of recoverable heat to heat rejected from power cycle,[14] η_w	0.80
Power cycle efficiency relative to Carnot's, λ_e	0.5
Heat source operating temperature T_f	
in winter	500°C
in summer	800°C

Heat Pump

Nominal cooling capacity (ARI conditions)	10 tons of refrigeration
Average coefficient of performance in heating mode,[15] P_h	2.85
Gross coefficient of performance in heating mode using[16]	
solar, $COP_{h,s}$	0.864
gas, $COP_{h,g}$	1.157
Average coefficient of performance in cooling mode[17] P_c	3.00
Gross coefficient of performance in cooling mode[18] by	
solar, $COP_{c,s}$	0.561
gas, $COP_{c,g}$	0.827

Energy Costs

Unit cost of gas energy,[19] C_g	2×10^{-5} \$/W
Unit cost of electrical energy	7×10^{-5} \$/W

[12] Selected based on the performance optimization given in Appendix B.

[13] Includes friction in bearings, coupling, lubricating oil pump, and other parasitics.

[14] Only required during the building heating mode.

[15] See Appendix C, and Table 2. Average P_h is taken from $\Sigma Q_{b,h}/\Sigma (Q_{b,h}/P_h)$.

[16] See Appendix B, Fig. 3, and Table 2. Average COP_h is taken from $\Sigma Q_{b,h}/\Sigma (Q_{b,h}/COP_h)$.

[17] See Appendix C, and Table 2. Average P_c is taken from $\Sigma Q_{b,c}/\Sigma (Q_{b,c}/P_c)$

[18] See Appendix B, Fig. 2, and Table 2. COP_c, on the average, is taken from $\Sigma Q_{b,c}/\Sigma(Q_{b,c}/COP_c)$.

[19] This amounts to \$0.60/Therm or \$6.00/Million Btu.

Other Economic Data	
• System life, N	15 years
• Annual interest rate on borrowed money, i	10%
• Capital recovery factor,[20] CRF	0.13147
• Hardware and installation costs of:	
• Heat pump[21]	$11,000
• Master control panel, plant start-up, duct work, motorized dampers, etc.	$ 8,000
• Power conversion module[22]	$ 3,000 - 10,000
• Solar collection subsystem[23]	$15,000 + (100 → 250) A_s
• Cost of alternate systems[24]	
• A nominal 20 kW_e electrical resistance heater	$1,000
• A nominal 20 kW (68,000 Btu/h) gas-fired heater	$2,000

The calculation procedure is summarized as follows:

(1) Because the calculations are made on representative days, one for each month, the daily average outside air temperature, T_o, and the direct normal solar radiation (required only for the 2-axis tracking collector) are tabulated for the site under investigation as in Table 1. Summer and winter seasons are distinguished by the average value of t_o as compared to a given reference temperature.

(2) Estimates are made for the constant sources of heat gain to a space, per unit floor area (m_b), and the rate of heat loss (or gain) to the exterior environment, n_b. Detailed back-up information appears in Refs. 13, 17, and 19. Different values of m_b and n_b could be estimated on a monthly basis; however, two changes, one for each season, are found satisfactory. Once the building's inside design temperature, t_i, is fixed, the heat gain to (or loss from) a space, Q_b, is calculated using Eq. (7). The results are listed in Table 2 and sketched in Fig. 11. A comparison of the outside air temperature and the changeover temperature, as obtained from Eq. (8), determines the mode of system operation . . . cooling or heating.

(3) The results of the coefficient of performance optimization versus the working fluid temperature from Appendix B, indicate that the changes in the optimum receiver-engine working temperature, T_f^*, has a minor effect on the optimum design point. Therefore, a working value of T_f, not necessarily the optimum value T_f^*, for each mode of operation should be chosen in advance, based either on average all-season conditions or on given metallurgical specifications. Monthly computations of P_c, P_h, R_c, R_h, E, COP_h and COP_c follow directly using Eqs. (C-7) and (C-12) of Appendix C and Eqs. (3), (4), (12), (13), (15), and (16).

(4) The monthly cost parameters β_s and β_b for both heating and cooling modes of operation, using Eqs. (18), (19), (21), and (22), are calculated next. The effective sun-tracking period, S, (assumed here as 80% of the daily sunshine period) is introduced to yield practical values for S. The price of the gas energy unit, c_g, is assumed to be representative for the time of the study. Energy cost escalation above general inflation is assumed the same as the escalation of the money interest rate above general inflation.

(5) Having determined the β coefficients, two approaches could be followed: the first approach is to graphically plot, as in Fig. 12, the yearly costs of energy, C_c, C_h, versus the area ratio A_s/A_b. Together with the levelized implementation and maintenance costs, the levelized total cost LTC could be plotted as shown in Fig. 13. For instance, two different concentrator costs were tried (C_s of 100 $/m^2$ and 150 $/m^2$ in addition to a $1500 basic cost). For each unit concentrator cost, C_s, the optimum size A_s^*/A_b differs and a graphical representation for each is necessary. The second approach in determining the optimum area ratio is nongraphical and slightly less accurate than the first approach, but yields faster results. The second approach utilizes the quadratic curve fit of C_c and C_h previously described in Section III-12. The resulting economic feasibility conditions are given by Eqs. (30) - (32). Numerically, Table 2 is constructed for the given sample building

[20] Calculated from Eq. (24).

[21] For a nominal 15 kW_e compressor, 10-ton unit, approximately $730/$kW_e$. Subtract $1,000 if the heat pump operates only as a chiller.

[22] Smaller figure represents the projected mass production cost ($200/$kW_e$). The large figure represents current cost of units under development.

[23] To include costs of paraboloid mirror, receiver, storage, structure and foundation. It consists of a fixed cost and a variable part C_s depending on the solar collector area A_s in m^2.

[24] To be used in conjunction with Table 3.

following the above steps. The key quantities which appear in Eq. (30) are found as

$A_b = 304\ m^2$ $\quad CRF = 0.13147$

$\sum_{M_c} \beta_{b,c} = 3.5291\ \$/m^2$ $\quad \sum_{M_h} \beta_{b,h} = 2.0311\ \$/m^2$

$\sum_{M_c} \beta_{s,c} = 18.236\ \$/m^2$ $\quad \sum_{M_h} \beta_{s,h} = 18.011\ \$/m^2$

$\bar{A}_{s,h}/A_b = 0.245$ $\quad \bar{A}_{s,c}/A_b = 0.332$

For a unit concentrator cost C_s of 100 $\$/m^2$, (A_s^*/A_b) is 0.1845, from Eq. (30), which if compared to 0.19 using a graphical solution, gives a good test to Eq. (30). At C_s of 150 $\$/m^2$, Eq. (30) also gives (A_s^*/A_b) as 0.132 vs 0.12 if a graphical solution is made. This deviation is not large considering a faster engineering assessment. A maximum C_s for any economically feasible solution where $A_s^* > 0$ is also obtained from Eq. (31) as 276 $\$/m^2$, i.e., the total concentrator cost should not be more than $(1500 + 276\ A_s)$ \$. Using the fitted coefficients $(a_{1,c} + a_{1,h})$, $(a_{2,c} + a_{2,h})$ and $(a_{3,c} + A_{3,h})$ from Eqs. (27) - (29) as 5.5602, -36.2467, and 62.5892, respectively, the fitted $(C_c + C_h)$ curve is plotted as the dotted line in Fig. 13, to show the difference between the graphical and analytical approaches. The fitted curve is only valid for $A_s/A_b \leqslant 0.245$, which satisfies the peak heating load.

V. Summary of Results

The work described in this first assessment of solar-assisted gas-fired heat pumps has been initiated to benefit the DSN facility in regard to enhancing its performance. The work could be briefly summarized as follows:

(1) A complete air-air heat-pump system powered by a dual heat source has been outlined. Major system components have been identified and a breakdown of energy and flow streams given. Analytical expressions have been provided for the optimization of solar concentrator size at a minimal total system cost.

(2) For a selected office-type building located at the DSN Communication Complex at Goldstone, California, monthly load computations, modes of system operation, and component performance efficiencies have been determined for a given heat-pump size. The results of this step have been used to compute the yearly energy cost with and without a solar collection subsystem.

(3) The larger the solar concentrator size, the more gas energy will be displaced by solar energy, thus reducing the yearly energy cost and, on the other hand, increasing the implementation cost. The levelized total cost combining implementation, maintenance, and operation costs, will have a minimum value at the optimum collector area. This is shown graphically and analytically.

(4) The levelized total cost is sensitive to the concentrator cost per unit area, and if the latter ranges under a mass production program from 100 to 150 $\$/m^2$, the optimum concentrator area ratio A_s^*/A_b will be on the order of 0.19 to 0.12, respectively. No solar connection is found to be economical if the concentrator cost exceeds 275 $\$/m^2$. For instance, at a concentrator cost of 100 $\$/m^2$, the optimum concentrator size $(A_s^*/A_b = 0.19)$ provides 91% of the building's heating during the year and 72% of the building's cooling load for the year. Favorable economics are evident if the concentrator cost decreases and the gas energy cost increases further.

To supplement the engineering assessment of the proposed heat-pump dual heat-source concept, four alternate systems are compared in Table 3. Each is designed to provide the same heating and cooling needs for the selected building. The alternate systems are: (a) an all-electric system with an electrical resistance heater and a vapor compression chiller, (b) a combined gas-electricity system with a gas-fired heater and a vapor compression chiller, (c) an all-electric system using a heat pump for both heating and cooling, (d) an all-gas system using a gas-engine-driven heat pump. The proposed solar-assisted gas-engine driven heat pump is simply a superimposed feature on the alternate system (d). By a simplified 10-year life-cycle cost analysis including an energy escalation rate only 10% higher than that of money interest, system (a) was the highest and systems (b), (c), and (d) were found to be of comparable cost. A cost refinement for all systems (b), (c), and (d) requires detailed cost information that is of secondary importance as far as system-selection is concerned at this stage of the assessment.

The solar-assisted system under study possesses several advantages over other direct solar-heating or cooling devices, such as: 1) the elimination of large thermal energy storage, since gas combustion could run the system instantaneously during cloudy hours, or during nighttime, and 2) the close proximity of the power cycle and the conditioned space, which makes the utilization of rejected heat more feasible, and almost doubles the heat-pump performance. This results in a low total-energy cost. The field implementation, however, needs to satisfy other developmental, environmental and economic constraints that are currently being investigated.

References

1. Calm, J. M., and Bauer, P. T., "District Heating and Cooling with Heat Pump System," paper No. 799357, presented at the 14th IECEC Conference, Boston, Mass., August 1979, pp. 1681-1686.
2. Yudow, B. D., et al, "Feasibility of a Heat-Actuated Heat-Pump-Centered Integrated Community Energy System," paper No. 799358, presented at the 14th IECEC Conference, Boston, Mass., August 1979, pp. 1687-1692.
3. Lior, N., "Solar Rankine Cycle (steam) Drive and Assistance to Heat Pump Systems," paper presented at the Solar Energy Heat Pump Systems for Heating and Cooling Buildings, Pennsylvania State University, June 1975, ERDA document C00-2560-1.
4. Sullivan, D., "Technology Impact Study of a High Efficiency Industrial Heat Pump," paper No. 799365, presented at the 14th IECEC Conference, Boston, Mass., August 1979, pp. 1725-1929.
5. Wurm, J., "Assessment of Selected-Engine Driven Heat Pumps," presented at the Solar Energy Heat Pump System for Heating and Cooling Buildings, Pennsylvania State University, June 1975, ERDA Document C00-2560-1.
6. Biancardi, R. F., and Meader, M. D., "Demonstration of a Turbocompressor Air Conditioning System," paper presented at the Solar Energy Heat Pump Systems for Heating and Cooling Buildings, Pennsylvania State University, June 1975, ERDA Document C00-2560-1.
7. Fischer, R. D., et al., "A Solar Heat Pump Featuring Pivoting-Tip Vanes," paper presented at the Solar Energy Heat Pump Systems for Heating and Cooling Buildings, Pennsylvania State University, June 1975, ERDA Document C00-2560-1.
8. Barber, R. E., "Solar Rankine Engines—Examples and Projected Costs," an ASME paper presented at the Gas Turbine Conference, San Diego, Calif., March 1979.
9. Allen, R. A., and Stiel, L. I., Working Fluids for Solar Rankine Heat Pumps," presented at the Solar Energy Heat Pump Systems for Heating and Cooling Buildings, Pennsylvania State University, June 1975, ERDA Document C00-2560-1.
10. Richards, W. D., and Chiu, W. S., "System Performance of a Stirling Engine-Powered Heat Activated Heat Pump," paper No. 799359, presented at the 14th Intersociety Energy Conversion Engineering Conference (IECEC), August 1979, pp. 1693-1698.
11. Patani, A., and Bonne, U., "Modeling the Performance of Gas-Fired Heat Pump Systems," paper No. 799360, presented at the 14th IECEC Conference, Boston, Mass., August 1979, pp. 1699-1707.
12. Martini, W. R., "An Efficient Stirling Heat Engine-Heat Pump," presented at the Solar Energy Heat Pump Systems for Heating and Cooling Buildings, Pennsylvania State University, June 1975, ERDA Document C00-2560-1.
13. Stamper, E. and Koral, R. L., editors, *Handbook of Air Conditioning, Heating and Ventilating*, Third Edition, Industrial Press, Inc., N. Y., 1979, Section 3.
14. Ekroth, I. A., "Thermodynamic Evaluation of Heat Pumps Working With High Temperatures," paper No. 799363, presented at the 14th IECEC Conference, Boston, Mass., August 1979, pp. 1713-1719.
15. Freeman, T. L., et al., "Computer Modeling of Heat Pumps, and the Simulation of Solar-Heat Pump Systems," ASME paper No. 75-WA/SOL-3, presented at the ASME Winter Annual Meeting, Houston, Texas, November 1975.

16. American Society of Heating, Refrigeration and Air Conditioning Engineers (ASHRAE) Guide and Data Book, 1972, Ch. 43.

17. Lansing, F. L., "A Sensitivity Model for Energy Consumption in Buildings," *TDA Progress Report 42-61*, Jet Propulsion Laboratory, Pasadena, Calif., pp. 58-87, February 1981.

18. Elliot, D. G., "Design and Economics of Solar Cooling for Electrically Powered Southern California Buildings," publication No. 5030-186, Jet Propulsion Laboratory, Pasadena, Calif., March 1978.

19. *Handbook of Fundamentals*, American Society for Heating, Refrigeration and Air Conditioning Engineers (ASHRAE), N. Y., N. Y., 1972.

20. Kusuda, T. and Ishii, K., "Hourly Solar Radiation Data for Vertical and Horizontal Surfaces on Average Days in the United States and Canada," NBS Building Science Series, 96 NBS, U. S. Dept. of Commerce, April 1977.

21. Rapp, D. *Solar Energy*, Prentice-Hall, Inc., N. J. 1981, Chapter 9.

22. Barnett, R. C., "Performance Characteristics of Air-to-Air Heat Pumps," presented at the Solar Energy Heat Pump Systems for Heating and Cooling Buildings, Pennsylvania State University, June 1975, ERDA Document C00-2560-1.

23. Miller, J. F., "Extended Range Water Source Heat Pumps," presented at the Solar Energy Heat Pump Systems for Heating and Cooling Buildings, Pennsylvania State University, June 1975, ERDA Document C00-2560-1.

24. Trelease, S. W., "Water Source Heat Pump Evaluation," *Heating, Piping, & Air Conditioning Journal*, October 1980, pp. 75-85.

Definition of Symbols

A	Projected area, m^2
a	cost coefficient, $\$/m^2$
C	cost, \$
CC	cooling capacity of a heat pump, tons of refrigeration
COP	Gross coefficient of performance
CRF	Cost recovery factor
E	Efficiency of energy conversion subsystem
F	Flow factor in solar receivers
I	Solar intensity, W/m^2
i	Interest rate on borrowed money, %
LTC	Levelized total cost, \$
M	Time in months of a given mode of operation
m	Intercept of a straight line
N	System life in years
n	Slope of a straight line
P	Coefficient of performance of heat pump subsystem
Q	Thermal energy per unit floor area, W/m^2
R	Solar concentrator-receiver efficiency
S	Effective daily solar radiation input, Whr/m^2 day
t	Temperature °C
T	Absolute Temperature, K
U	Heat loss coefficient for solar receiver, $W/m^2°C$
ρ	Spectral reflectivity of concentrator surface
ϕ	mirror-receiver intercept factor
η	efficiency
α	effective absorptivity of solar receiver
β	cost parameter, $\$/m^2$
θ	dimensionless parameter
λ	fraction of a corresponding Carnot's cycle

Superscripts

$-$	peak or design conditions
$*$	changeover/optimum conditions

Subscripts

b	building
c	cooling mode
co	condenser
e	heat engine or power conversion subsystem
ev	evaporator
f	working fluid in solar receiver (or gas combustor)
g	gas combustor
h	heating mode
H	high temperature heat reservoir
i	inside the space
im	implementation
m	maintenance
L	low temperature heat reservoir
o	outside environment to space
s	solar-powered mode/solar concentrator
t	energy transmission and storage subsystem
w	waste heat recovery subsystem

Table 1. Monthly average weather parameters for Goldstone, California

Month	Direct solar radiation data[a]				Daily average outside air temperature, T_o, °C	Season[b] S = summer W = winter
	Noon intensity, I_n, W/m^2	Daily input, Wh/m^2, day	Sunny hours, h/day	Average intensity over the sunny, I, hours, W/m^2		
Jan	960	7473	8	934	6.4	W
Feb	987	8697	10	870	11.1	W
Mar	980	9399	10	940	12.1	W
Apr	933	9732	12	811	14.3	W
May	901	9880	12	823	19.8	S
Jun	883	9799	12	817	26.1	S
Jul	876	9564	12	979	29.7	S
Aug	890	9180	12	765	29.1	S
Sep	928	8751	10	875	24.4	S
Oct	949	8246	10	825	17.4	W
Nov	943	7301	8	913	10.7	W
Dec	940	7042	8	880	5.3	W
Average for 5 summer months		9435	10	943	25.8	S
Average for 7 winter months		8270	8.4	880	11.0	W

[a]Uses ASHRAE model (Refs. 19 and 20).
[b]Classified as summer or winter depending on whether the average daily outside air temperature is higher than or less than 18.33°C, respectively.

Table 2. Monthly results of the sample office building

Month	t_o[a], °C	Season[a]	t_i, °C	Q_b[b], W/m^2	Mode[c] of operation	P	T_f, °C	COP_g[d]	COP_s[e]	S[f] Wh/m^{2}day	β_b[g]	β_s[g]
May	19.8	S	25.56	9.45	C	3.813	800	1.059	0.710	7904	0.1303	3.2237
Jun	26.1	S	25.56	39.58	C	3.117	800	0.858	0.576	7839	0.6735	3.2014
Jul	29.7	S	25.56	56.80[h]	C	2.782	800	0.764	0.536	7651	1.0854	3.2654
Aug	29.1	S	25.56	53.93	C	2.835	800	0.779	0.514	7344	1.0108	2.9478
Sep	24.4	S	25.56	31.45	C	3.289	800	0.908	0.620	7001	0.5057	2.9081
Oct	17.4	W	22.22	8.64	C	3.660	800	1.022	0.685	6597	0.1234	2.6898
Nov	10.7	W	22.22	-23.40	H	2.878	500	1.161	0.869	5841	0.2943	2.6596
Dec	5.3	W	22.22	-49.23[h]	H	2.810	500	1.150	0.855	5634	0.6250	2.5482
Jan	6.4	W	22.22	-43.97	H	2.841	500	1.156	0.867	5978	0.5553	2.7275
Feb	11.1	W	22.22	-21.49	H	2.883	500	1.162	0.864	6958	0.2700	3.1473
Mar	12.1	W	22.22	-16.70	H	2.896	500	1.165	0.876	7519	0.2093	3.4394
Apr	14.3	W	22.22	- 6.18	H	2.925	500	1.169	0.861	7786	0.0772	3.4885

[a]From Table 1 data.
[b]Calculated monthly from Eq. (7).
[c]C = cooling, h = heating, according to sign of Q_b.
[d]Using Eqs. (13), (16), Table 1, and Appendices B, C.
[e]Using Eqs. (12), (15), and Appendices B, C.
[f]Taking 80% of available solar radiation values in Table 1.
[g]Using Eqs. (18), (19), (21), and (22).
[h]Peak loads needed for equipment design.

Table 3. Comparison of alternate HVAC systems without a solar coupling

HVAC systems		System 1 Electrical resistance heating and electrical-powered chillers	System 2 Gas-fired heater and electrical-powered chillers	System 3 Electrical-powered heat pump for both heating and cooling	System 4 Gas-fired turbo-compressor heat pump
Annual[a] building load, kWh/yr	heating	← 35,722 →			
	cooling	← 44,351 →			
Average efficiency or COP of heating equipment		0.9[b]	0.85[b]	2.85[b]	1.157[d]
Average COP of cooling equipment		3.00[c]	3.00[c]	3.00[c]	0.827[d]
Itemized energy cost[e] per year, $	heating	2,778	840	877	617
	cooling	1,034	1,034	1,034	1,073
Yearly energy cost, $		3,812	1,874	1,911	1,690
Initial cost, $\times 10^3$ $		19[f]	20[g]	19[h]	22[i]
Approx. 10-yr life cycle[j] cost $\times 10^3$ $		79.75	49.87	49.46	48.93

[a] Using building loads from Table 2, 304 m^2 floor area.
[b] Assumed values.
[c] Averaged from Table 2 as $\Sigma Q_b/\Sigma (Q_b/P)$.
[d] Averaged from Table 2 as $\Sigma Q_b/\Sigma (Q_b/COP_g)$.
[e] Based on 2¢/kWh for gas heating and 7¢/kWh for electricity.
[f] $1K for heater, $8K for ducts, controls and $10K for a chiller.
[g] $2K for a boiler, $8K for ducts, controls and $10K for a chiller.
[h] $11K for a heat pump, $8K for ducts and controls.
[i] Same as system 3, add $3K for gas engine.
[j] With 10% energy escalation rate.

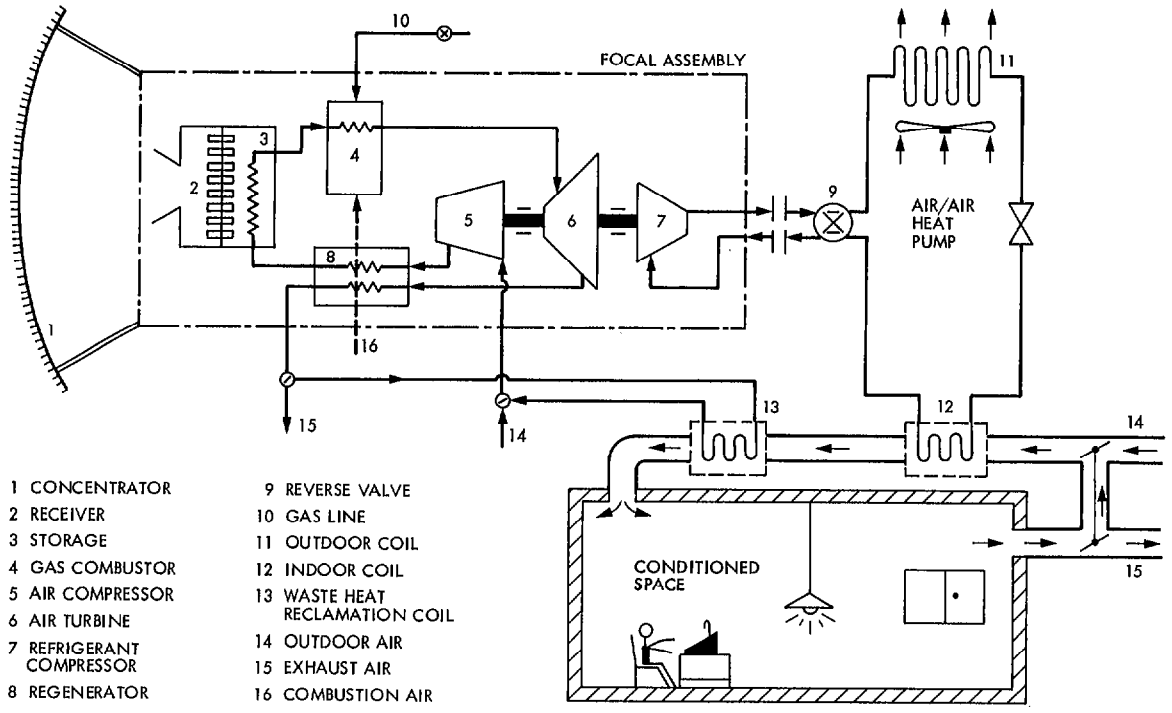

Fig. 1. Layout of a solar-assisted gas-fired heat-pump system (not to scale)

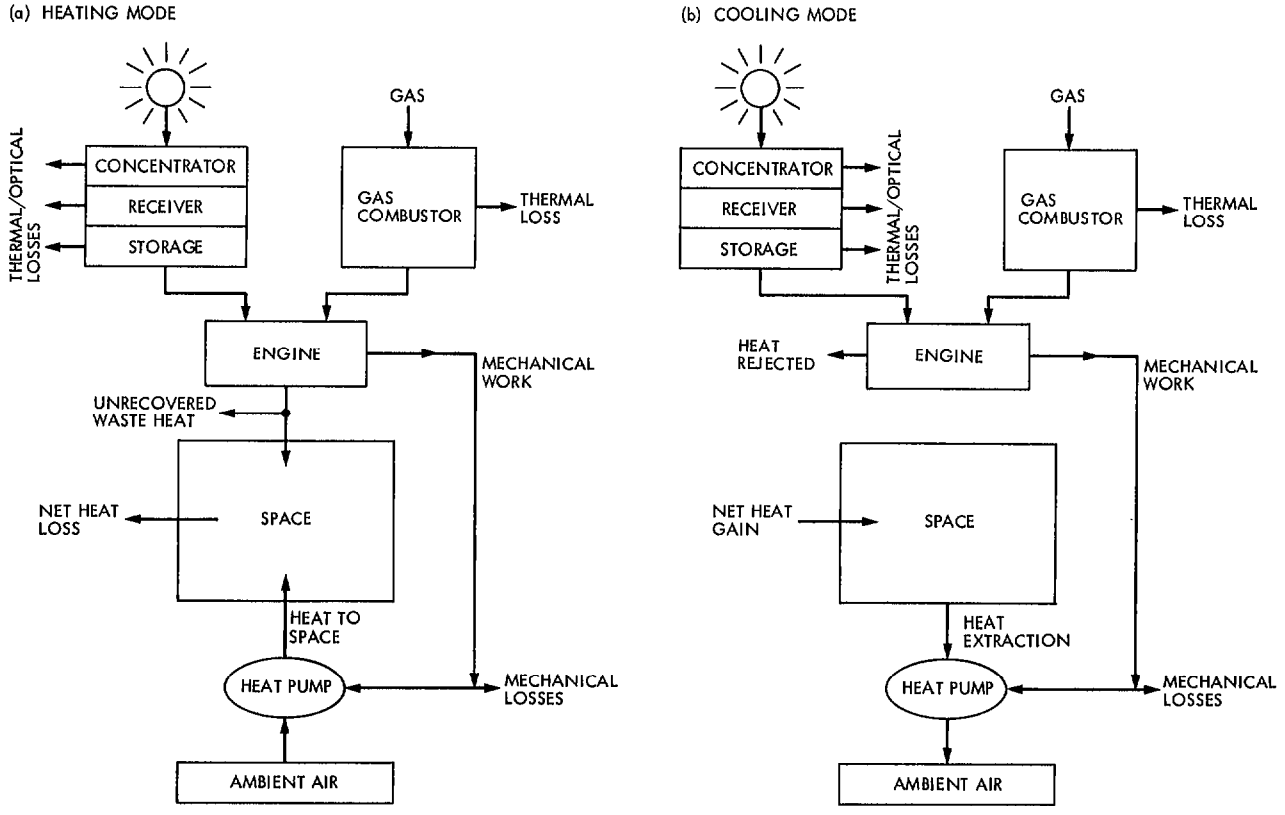

Fig. 2. System energy balance during modes of operation

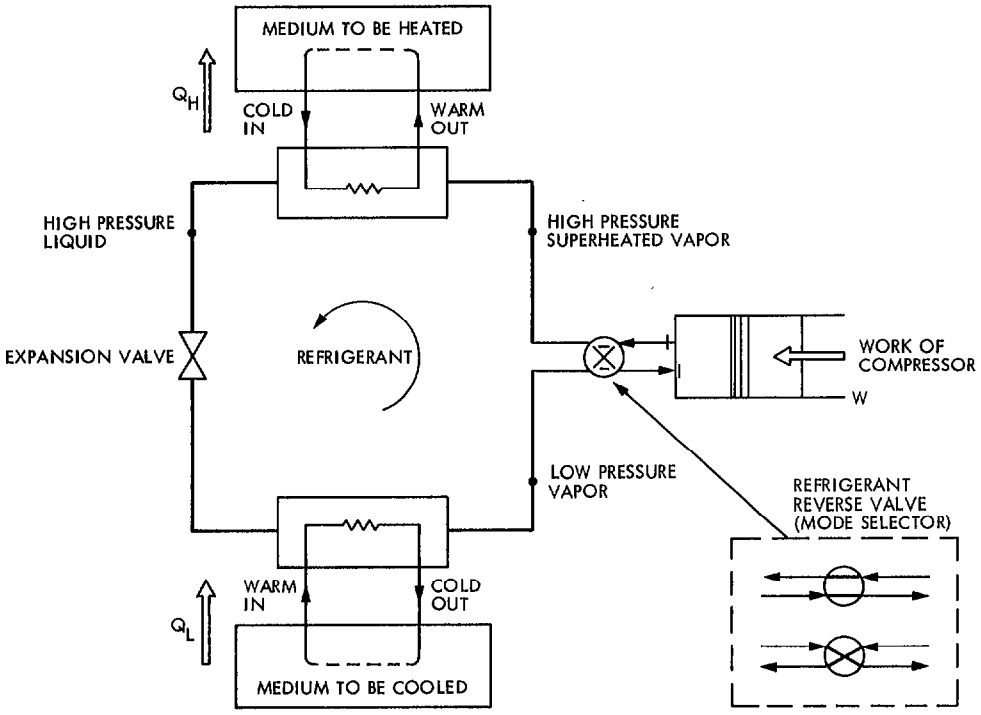

Fig. 3. Principle of operation of a heat pump

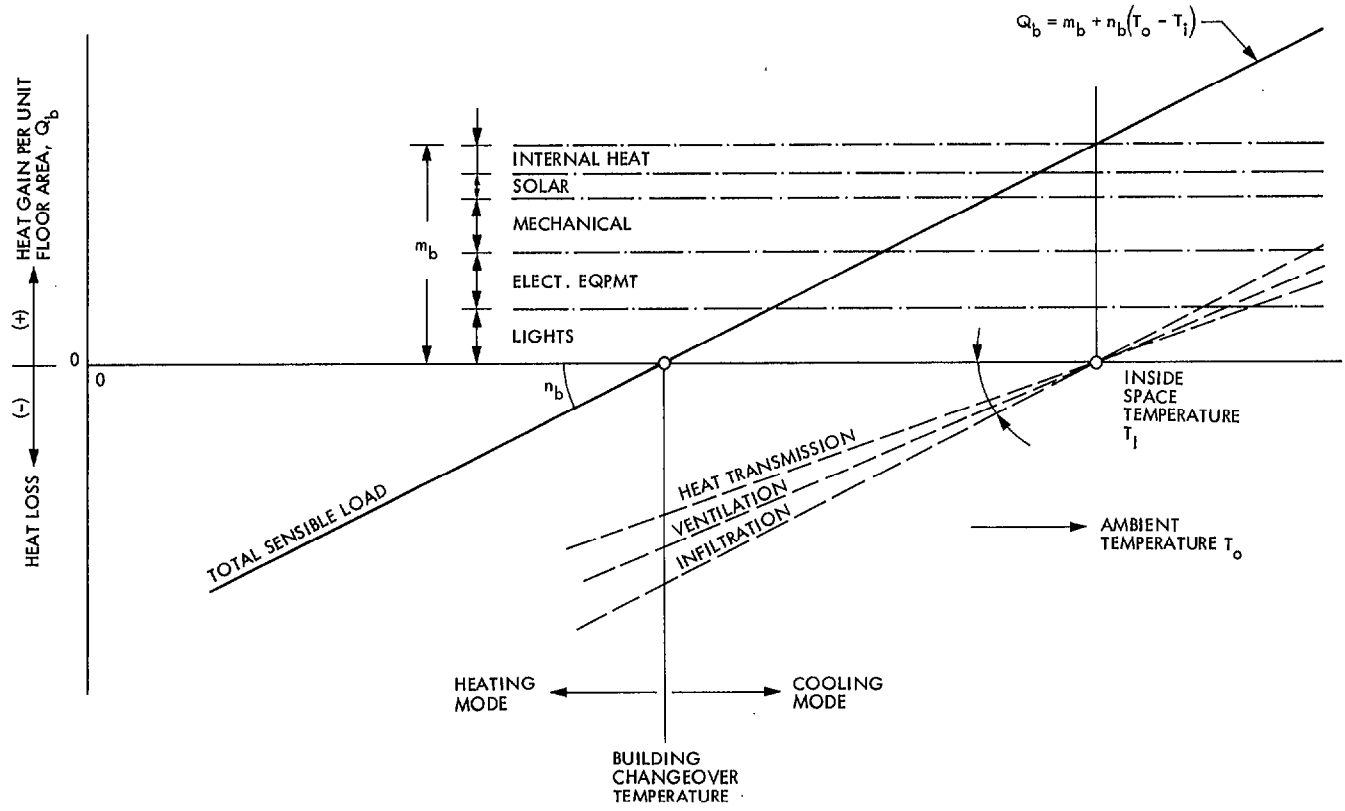

Fig. 4. General daily load profile for buildings

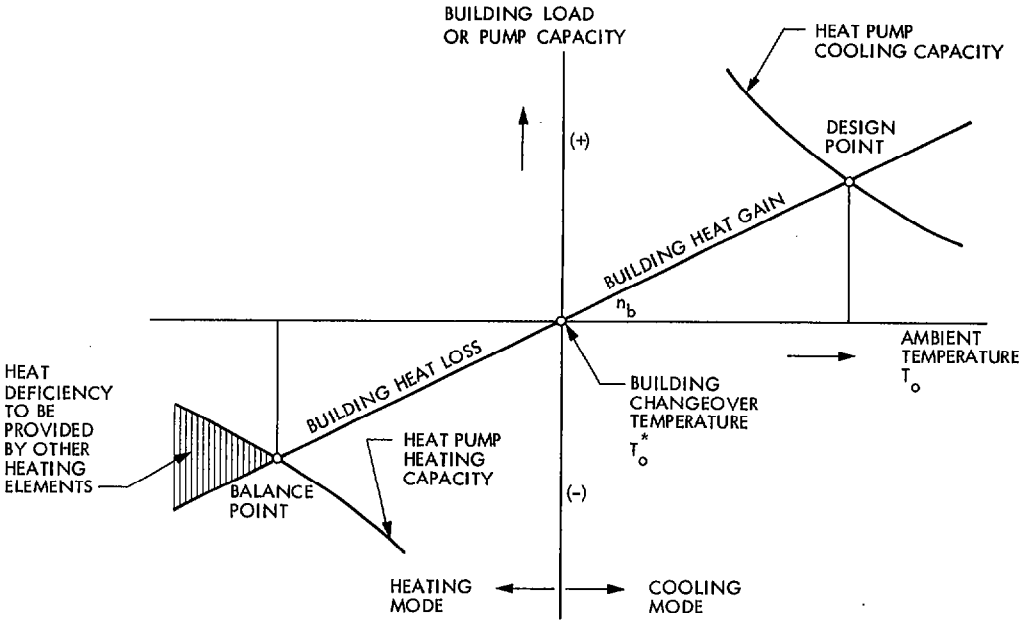

Fig. 5. Heat-pump capacity versus building load

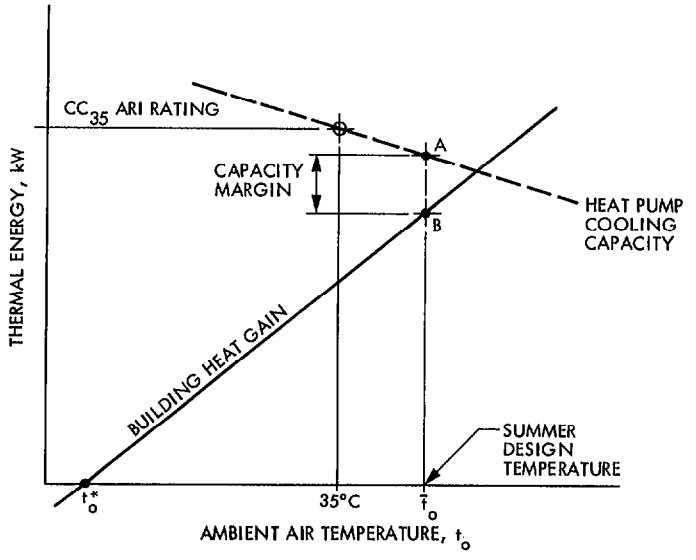

Fig. 6. Relationship between heat-pump capacity and building size at the design point

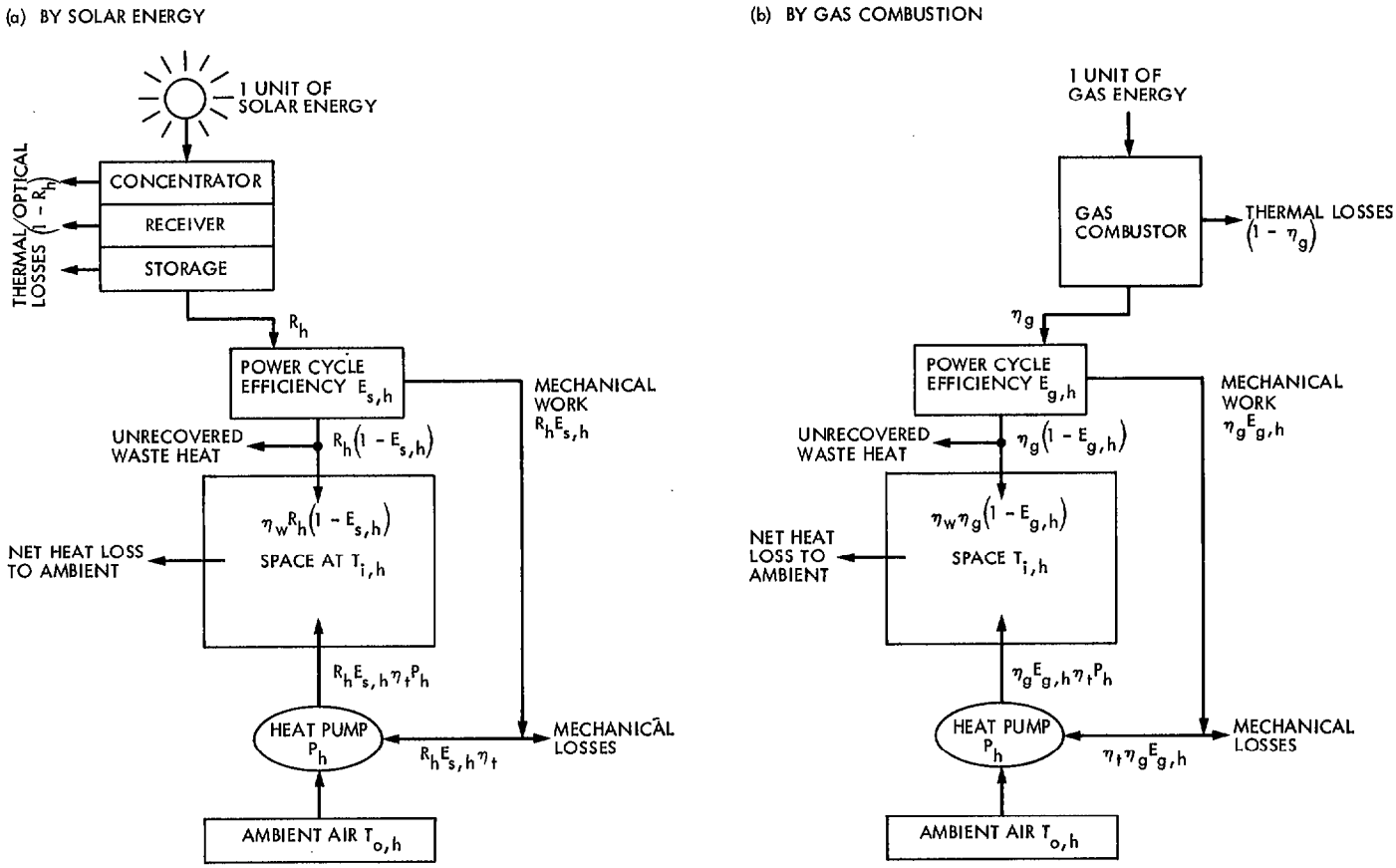

Fig. 7. Gross coefficient of performance during heating mode

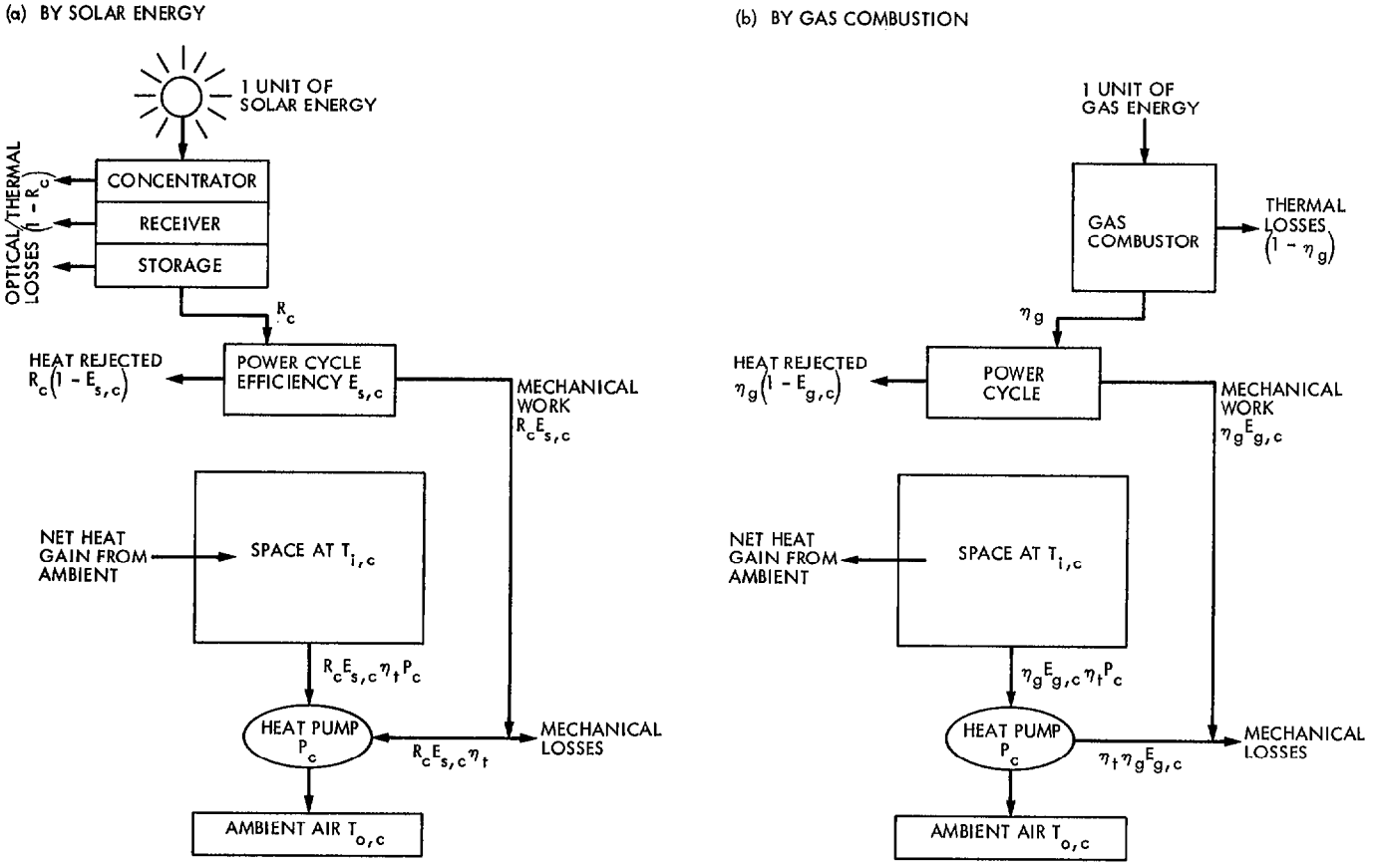

Fig. 8. Gross coefficient of performance during cooling mode

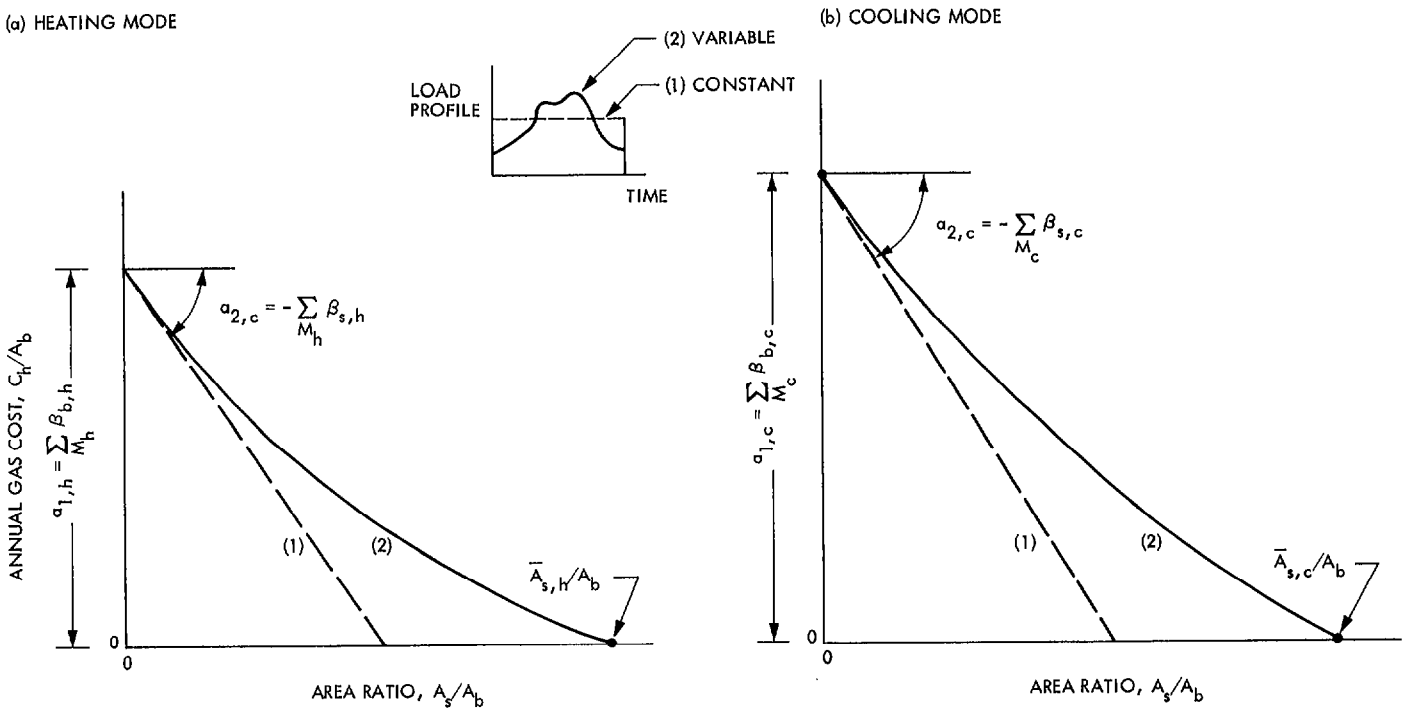

Fig. 9. Trends of gas cost versus solar concentrator area in both heating and cooling modes

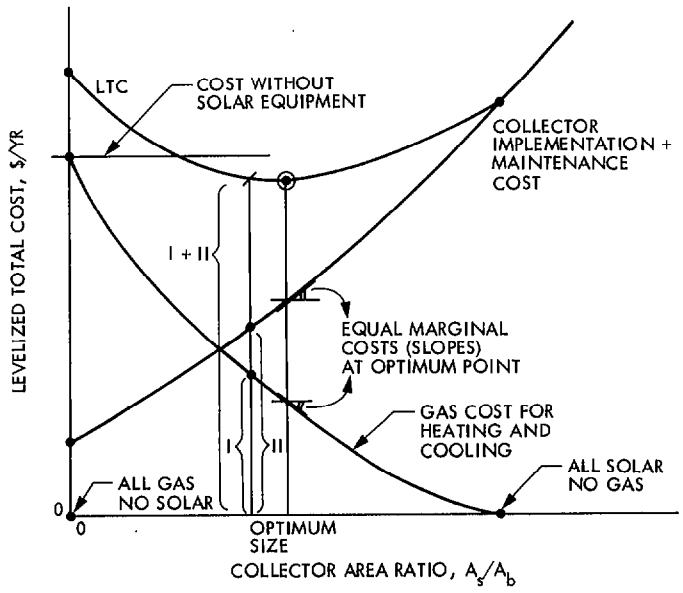

Fig. 10. The search for optimum concentrator size

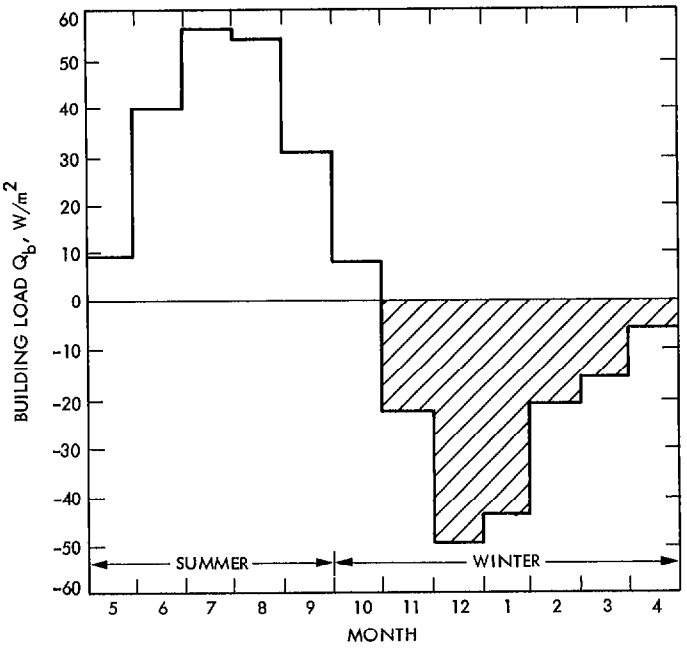

Fig. 11. Monthly heat gain (or heat loss) profile for the sample office building

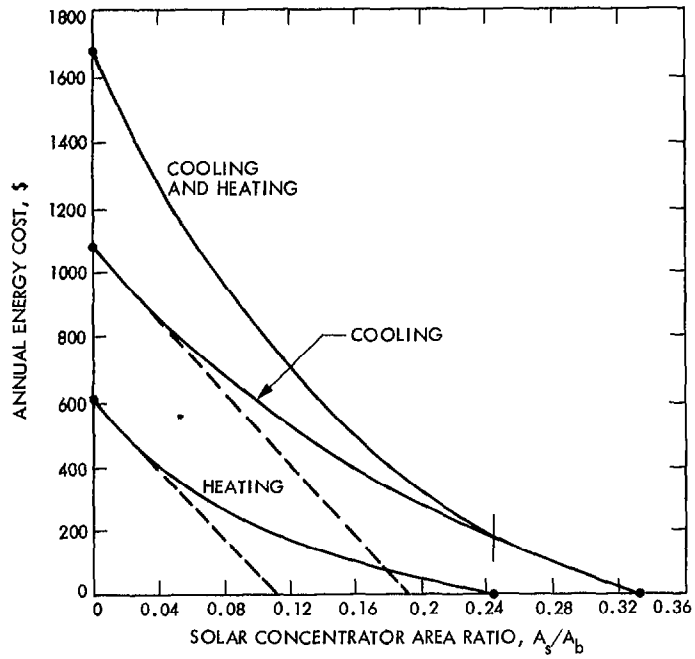

Fig. 12. Results of gas energy costs at different concentrator sizes for the sample building

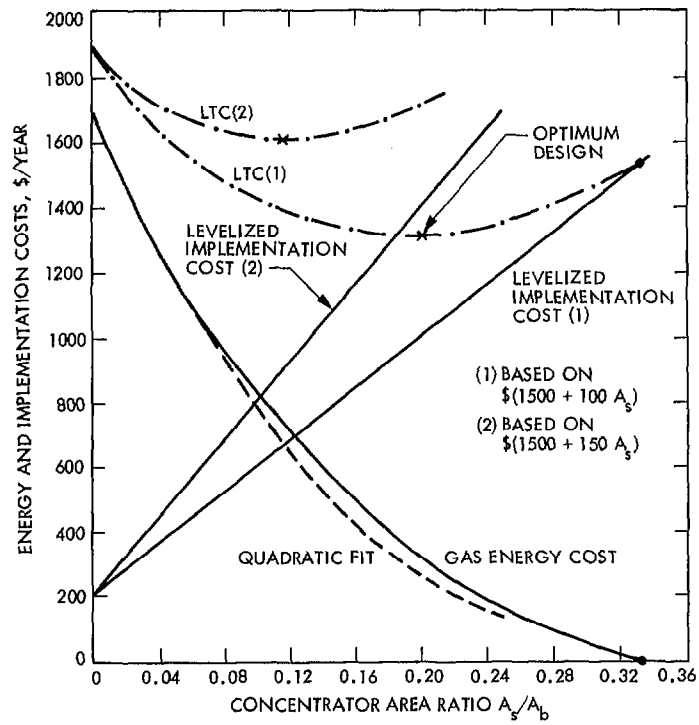

Fig. 13. Solar concentrator optimization for the sample building

Appendix A

Heat Pump Configurations

Four different types of heat pumps are generally available, which are classified basically according to the type of medium in contact with the refrigerant in either the indoor or outdoor elements. This medium acts as a heat source or a heat sink during operation. The heat pump classification is as follows:

(1) Air-to-air heat pump (A-A)

(2) Water-to-water heat pump (W-W)

(3) Water-to-air heat pump (W-A)

(4) Air-to-water heat pump (A-W)

The first medium always represents the outdoor fluid in contact with the refrigerant in the outdoor heat exchanger. This first medium acts either as a heat source (in a heating mode) or as a heat sink (in a cooling mode). The second medium is the indoor fluid which comes in contact with the refrigerant in the indoor heat exchanger. Consequently, the second medium acts either as a heat sink (in a heating mode) or as a heat source (in a cooling mode) (Refs. 13 and 21). Each of the above four heat-pump configurations is described briefly below.

I. Air-to-Air Heat Pump

This is the most widely used heat pump, and is illustrated in Fig. A-1 for both cooling and heating modes of operation with refrigerant reversing controls. (Ref. 22). Forced air, from fans, flows over both the indoor and outdoor refrigerant coils. A complete system requires an indoor air distribution network (ducts) to supply filtered warm or cool air as needed. Operating the A-A heat pump in a heating mode where the outdoor air temperature is very low (less than 7°C or 45°F) may cause frost formation on the outdoor coils. Coil frosting impairs the pump effectiveness, since it blocks the air flow and presents several operational difficulties. One solution to this problem is to reverse the mode-selector valve to the cooling mode frequently and for a few minutes until the hot outdoor coil (operating then as a heat rejection element) melts the frost. Other solutions such as the use of electric-resistance heaters or taking advantage of other waste-heat sources could be used.

In multi-zone air conditioning where different zones make different heating or cooling demands simultaneously, the use of A-A heat pumps with an air changeover system is sometimes preferred instead of having a refrigerant changeover selector. In this air-changeover system, the flow of air is controlled by a dual-duct network accompanied by a set of motorized dampers to direct the air across the condenser coils for heating or across the evaporator coils for cooling before entering the air-conditioned space as shown in Fig. A-2. The refrigerant flow is not reversed, however, in this system. Depending on the relative magnitude of heating and cooling demands, the heat pump extracts low temperature heat from zones that require cold air and gives it at high temperature to those zones that require warm air. Although a good potential for energy conservation exists in this configuration because the heat pump partially acts as a heat reclamation device, the air changeover system has not been widely recognized.

A-A heat pumps are generally designed in integral packaged form with small tonnage (up to 30 tons of refrigeration (105 kW)) for residential or commercial applications (Ref. 13). Since water is not used, the maintenance and operation problems of piping, plumbing, fluid leakage, or corrosion do not exist, which generally results in low maintenance costs.

II. Water-to-Water Heat Pump

As illustrated in Fig. A-3, a water-to-water heat pump uses water from a well, lake, river, or any large body of water as either a heat source or a heat sink. Water is also used to exchange heat to and from the refrigerant in the indoor coil. W-W heat pumps have been less popular commercially than A-A types due to:

(1) A shortage of clean water supply in some populated areas; generally, water from wells is returned to the ground in order not to deplete underground water supplies.

(2) Low water quality of city water, which in general contains soluble minerals. Deposits on piping and heat exchangers cause scaling and fouling; soft water, on the other hand, without some mineral content, can be corrosive.

(3) Plumbing costs could increase the first cost of the system.

In spite of the above operation and maintenance problems of W-W heat pumps, they offer several advantages over their competitors: They provide a higher coefficient of performance and less heat exchange surface area since water is a good heat transfer medium and, because of the constant temperature of well water, different from ambient air, they provide higher

performance during periods of peak heating (water temperature is higher than air temperature) or peak cooling (water temperature is lower than air temperature). These advantages result in W-W heat pumps being lower in operating cost than the comparable A-A type.

W-W heat pumps could also operate with either the refrigerant reversing valve as shown in Fig. A-2 or water reversing valves. In a water changeover system, the direction of water leaving the condenser and chiller (evaporator) is controlled by valves to provide heating or cooling to multiple zones as required. In general, the refrigerant control is preferred to avoid contamination of indoor coils with the external water supplies (from a river, lake, ocean, etc.), which may be chemically untreated.

III. Water-to-Air Heat Pumps (W-A)

This heat pump also uses well or lake water as a heat sink/source similar to W-W heat pumps, but the heat is delivered to the indoor coil through direct expansion of the refrigerant as shown in Fig. A-4. The W-A heat-pump system has the same basic problems as the W-W type in regard to water availability, quality, and its disposal. However, it operates with higher performance than an A-A system if enough water (at temperatures higher than 10°C (50°F)) is available (Refs. 23 and 24). A W-A system could operate with air-reverse controls to supply cold/warm air as needed or else use refrigerant reverse controls as shown in Fig. A-4. The advantages of low initial cost and low maintenance cost of A-A systems are still applied, since it is a hybrid system of the above A-A and W-W systems.

IV. Air-to-Water Heat Pumps (A-W)

This heat pump is the same as W-A type above, except it uses outdoor air as the heat source/sink and exchanges heat with the indoor coil through the use of clean water as a secondary medium, as shown in Fig. A-5. A-W systems have the same advantages and limitations as W-A units. Since warm/cold water piping replace the interior air duct work, corrosion problems, though not entirely eliminated, are less frequent than in W-W or W-A systems.

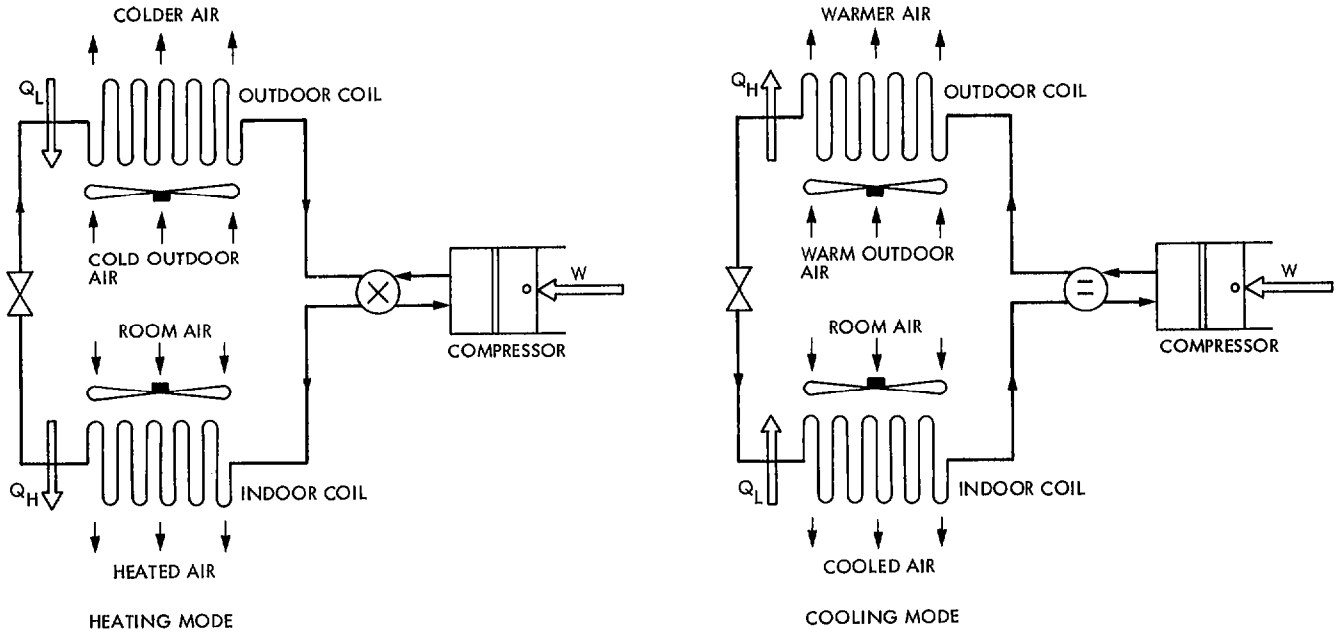

Fig. A-1. Air-to-air heat pump

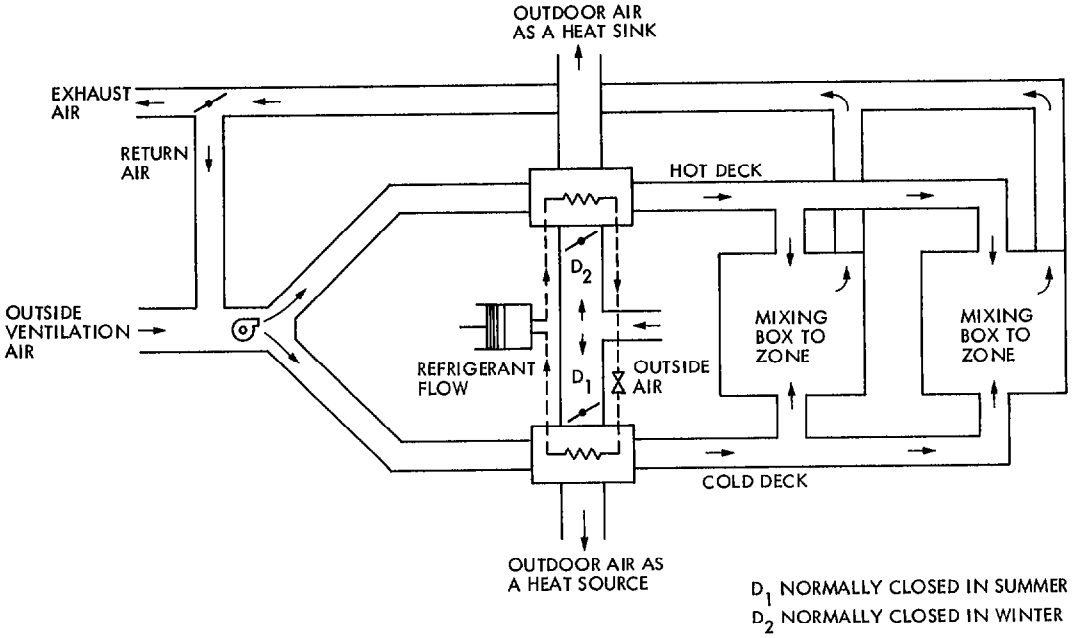

Fig. A-2. Multizone air-changeover A-A heat pump system with dual duct and mixing box controls

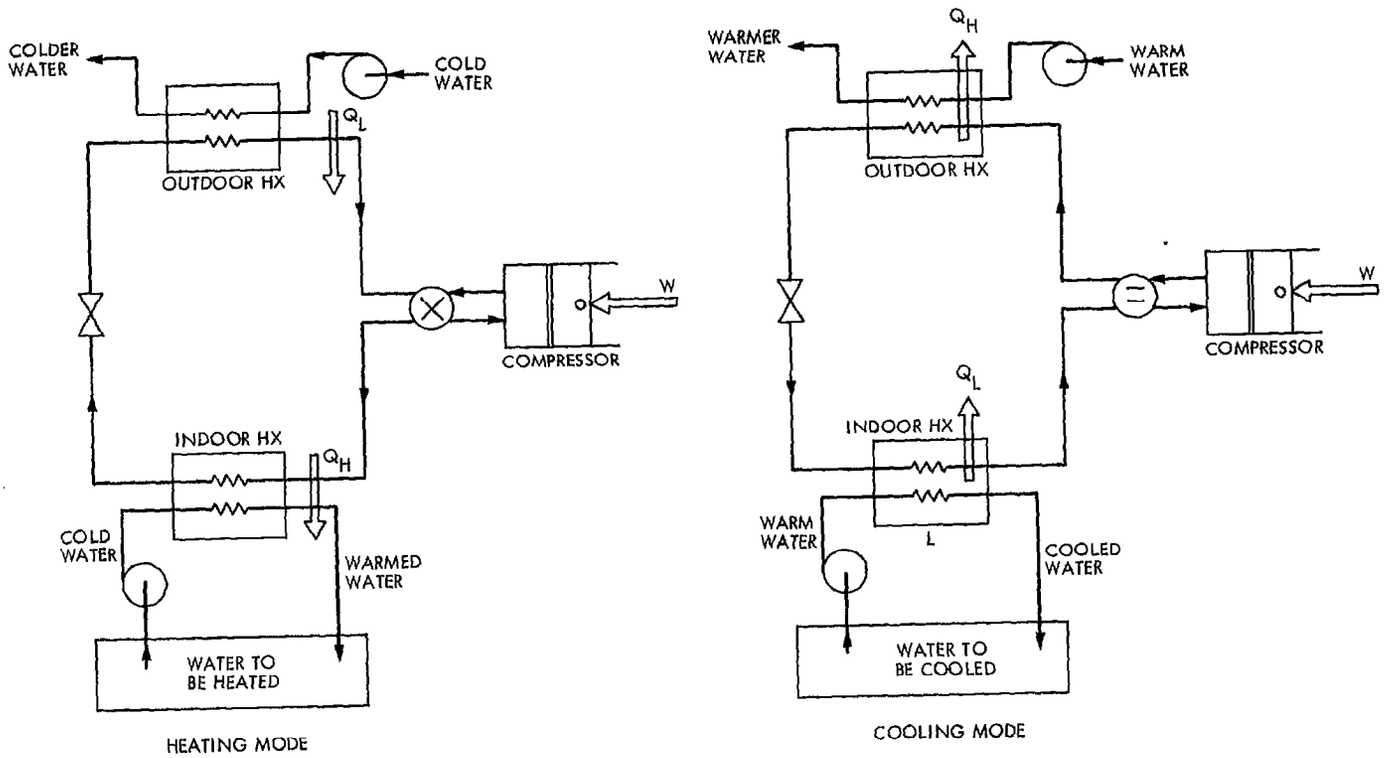

Fig. A-3. Water-to-water heat pump

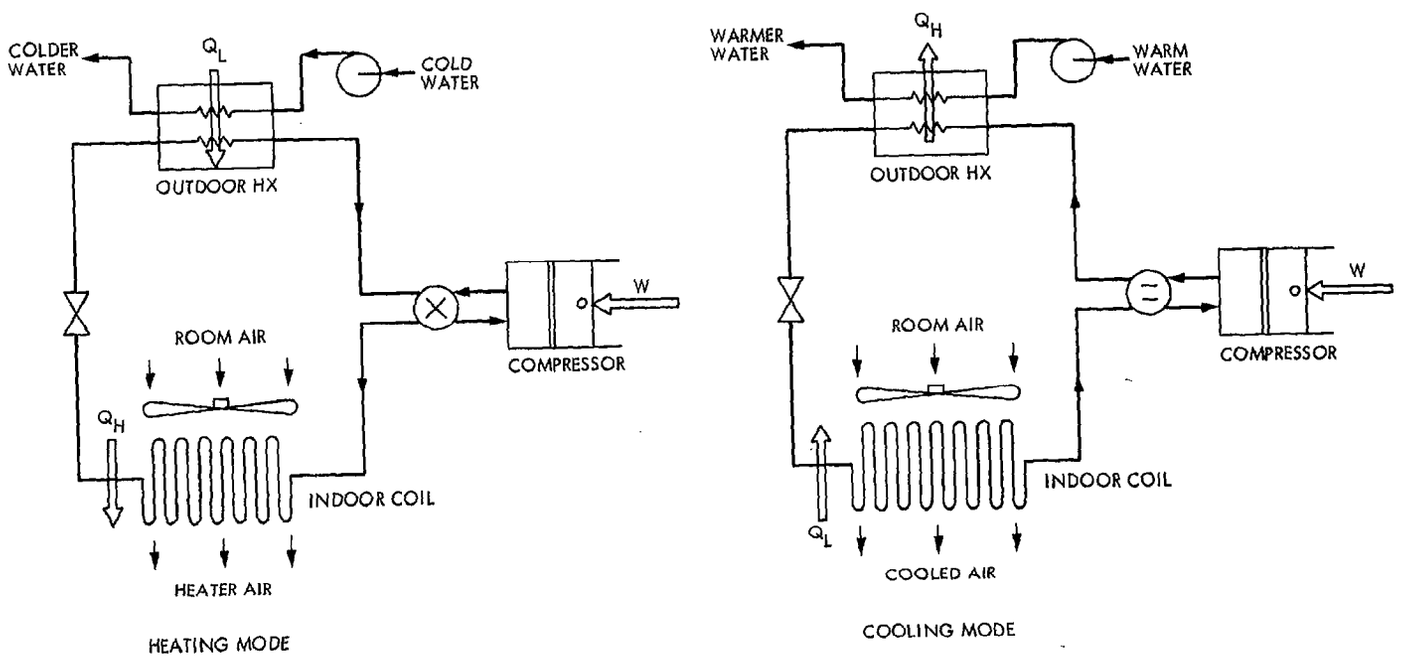

Fig. A-4. Water-to-air heat pump

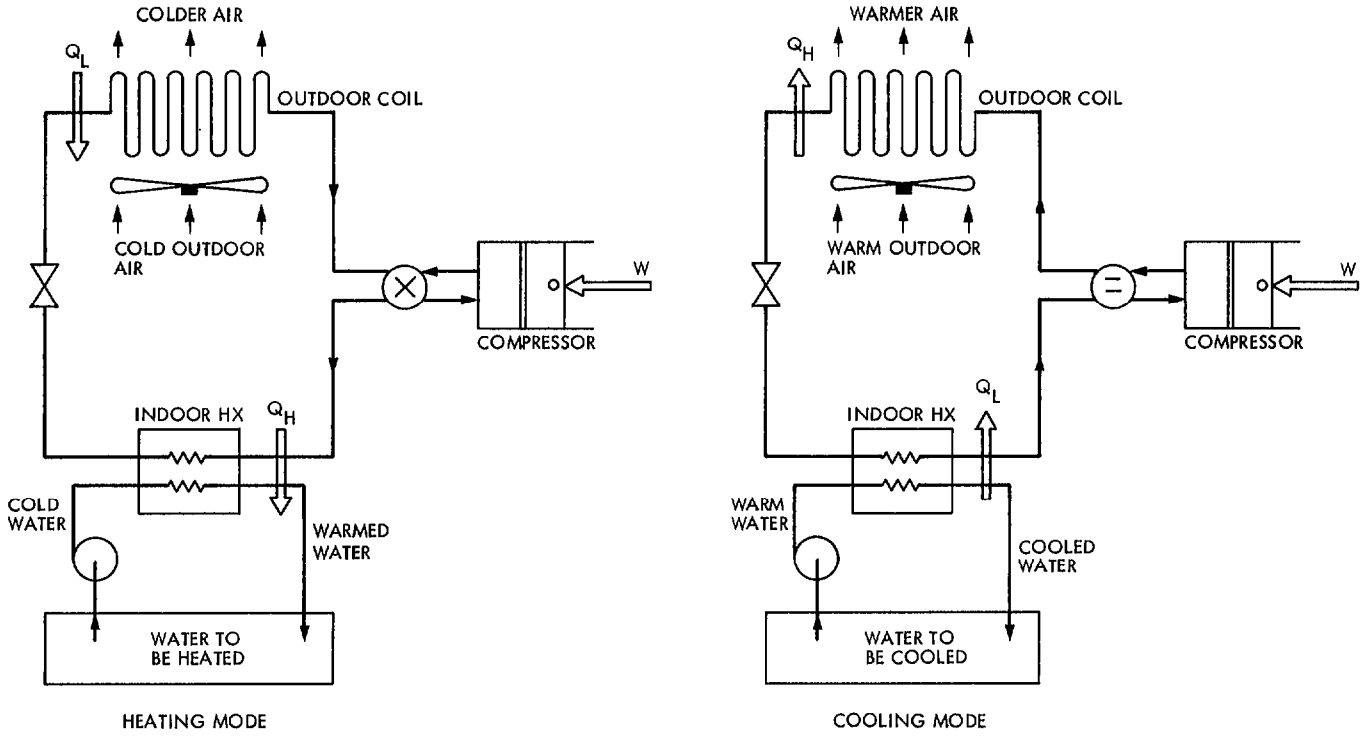

Fig. A-5. Air-to-water heat pump

Appendix B

Optimum Receiver-Engine Working Temperature

The operating temperature of the fluid circulating inside the solar receiver-storage subsystem is an important parameter in determining the coefficient of performance of the heat-pump system at any mode. In the cooling mode, and for a given solar-energy input, a high receiver temperature gives a high-power cycle efficiency, E, but results in a low collector efficiency, R, due to the increased receiver thermal losses. An optimum operating temperature is, therefore, required to maximize the product RE when operating in the cooling mode.

For the building-heating mode, the recoverable portion of the engine's rejected heat is also utilized as an additional heating effect to boost the basic heat-pump heating effect. For a given solar-energy input, the higher the receiver temperature becomes, the higher the power cycle efficiency E, the higher the heating effect by the heat pump, and the less the heat rejected from the engine. Again, an optimum receiver operating temperature is required to maximize the sum of the two heating effects. For each mode of operation, the optimum operating temperature is analyzed below, to enable the computations of P and COP expressions in the text.

I. Building Cooling Mode

According to Fig. 8(a), the coefficient of performance of the heat pump when operating during the sunny hours is given by:

$$COP_{s,c} = \eta_t \cdot P_c R_c E_{s,c} \tag{B-1}$$

Therefore, the procedure requires the maximization of only the product $R_c E_{s,c}$ with respect to the receiver fluid temperature T_f since the component efficients η_t, and P_c are independent of T_f. Note that the concentrator-receiver-efficiency R, is taken from Eq. (3) as

$$R = m_s - n_s \frac{(T_f - T_o)}{I} \tag{B-2}$$

where I is an hourly average solar intensity. The power cycle efficiency E, on the other hand, is simplified as a fraction of the corresponding Carnot's cycle when operating between the two temperature limits T_f as a heat source, and T_o as a heat sink. From Eq. (4),

$$E = \lambda_e \left(1 - \frac{T_o}{T_f}\right) \tag{B-3}$$

The maximum product RE, at the optimum fluid temperature T_f^*, is obtained by differentiation and by assuming m, n, T_o, I, and λ_e to be constants. The result is written as:

$$T_{f,c}^* = T_o \sqrt{1 + \frac{m_s I}{n_s T_o}} \tag{B-4}$$

A plot in Fig. B-1 of the quantities R, E, and RE versus T_f is also made for a selected numerical example. Figure B-1 illustrates that the maximum value of the product RE lies on a plateau and not on a sharp peak. For instance, the assigned values of $m_s = 0.722$, $n_s = 0.16$ W/m^2°C, $\lambda_e = 0.5$, $t_o = 25.8$°C (299 K), and $I_c = 943$ W/m^2, yield an optimum temperature T_f^* of 893°C and an optimum RE product of 21.4%. Operating the receiver-engine at 800°C (1472°F) instead of 893°C will yield an RE product of only 21.3%, which is an insignificant loss in performance compared to other cost and metallurgical gains obtained by lowering the operating temperature.

II. Building Heating Mode

When operating during the sunny hours, the gross coefficient of the heat-pump waste-heat recovery system is obtained from Fig. 7(a) as

$$COP_h = \eta_w R_h + R_g E_{s,h} (P_h \eta_t - \eta_w) \tag{B-5}$$

Upon the substitution of R and E expressions from Eqs. (B-2) and (B-3), respectively, and assuming that the component efficiencies η_w, P_h and η_t are independent of T_f, an optimum operating fluid temperature $T_{f,h}^*$ could be obtained by differentiation. The result is expressed as

$$T_{f,h}^* = T_o \sqrt{\left(1 + \frac{m_s I}{n_s T_o}\right)/\theta} \tag{B-6}$$

where θ, is a coupling parameter larger than or equal to 1, given by

$$\theta = 1 + \frac{\eta_w}{\lambda_e(P_h \eta_t - \eta_w)} \qquad \text{(B-7)}$$

Without utilization of any portion of the engine rejected heat, the efficiency η_w is zero, and the optimum temperature expression is reduced to Eq. (B-4). However, since θ is $\geqslant 1$, the temperature $T^*_{f,h}$ will always be less than $T^*_{f,c}$, keeping other parameters the same. Similarly to COP_c, the trend of COP_h changes very slowly with the temperature T_f, with an almost flat plateau around the optimum point rather than a sharp peak. The above finding allows the designer to choose a lower operating temperature for material consideration without a great sacrifice of the system performance. Numerically, Fig. B-2 is plotted for the same concentrator-receiver design ($m_s = 0.722$, $n_s = 0.16\ \text{W/m}^2\text{°C}$) under the average conditions of the site's winter season ($I_h = 880\ \text{W/m}^2$ $t_{o,h} = 11\text{°C}$) together with the assumed component efficiencies ($\eta_t = 0.9$, $\eta_w = 0.8$, $\lambda_e = 0.5$, $P_h = 2.88$) or at $\theta = 1.893$. The optimum $T^*_{f,h}$ is found to be 525°C (977°F), resulting in a maximum COP_h of 0.864. At the selected receiver-engine operating temperature of 500°C, the gross COP_h becomes 0.863, which gives a negligible difference in performance.

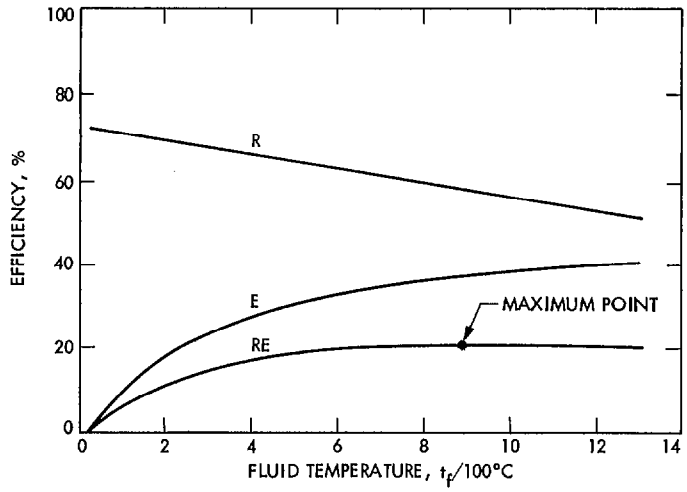

Fig. B-1. Optimum RE product in cooling mode

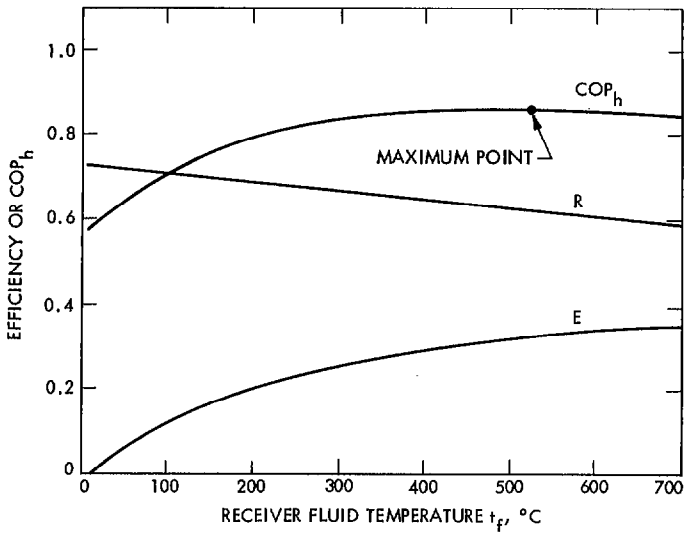

Fig. B-2. Optimization of the gross coefficient of performance during the solar-heating mode

Appendix C

Temperature Levels and Coefficient of Performance of Heat Pumps

Actual heat transfer in heat-pump components requires a temperature difference to transfer heat both from the heat source to the evaporating refrigerant and from the condensing refrigerant to the cooling fluid. Accordingly, the temperature span of the refrigeration cycle will increase over that cycle which is represented only by the heat-source and heat-sink temperatures. For each mode of operation, the temperature levels are here represented by empirical expressions in terms of source/sink temperatures instead of the graphical representation given in Ref. 16. For a direct comparison with the corresponding Carnot's refrigeration cycle, the procedure is discussed as follows.

I. Cooling Mode

The evaporator side temperature difference Δt_{ev}, as sketched in Fig. C-1, could be represented analytically by.

$$\Delta t_{ev} = 23.11 - 0.2\, t_o = t_i - t_{ev} \qquad \text{(C-1)}$$

hence

$$t_{ev} = t_i + 0.2\, t_o - 23.11 \qquad \text{(C-2)}$$

Similarly, the condensing side temperature difference, Δt_{co}, could be represented by:

$$\Delta t_{co} = 21.44 - 0.2\, t_o = t_{co} - t_o \qquad \text{(C-3)}$$

or

$$t_{co} = 21.44 + 0.8\, t_o \qquad \text{(C-4)}$$

An actual heat pump will be as efficient as roughly a fraction (between 40 to 60%) of the Carnot-cycle heat pump operating between T_{ev} and T_{co} (Ref. 16). If the fraction λ_c is approximated by the relationship, then

$$\lambda_c = 0.536 - 0.0058\, t_o \qquad \text{(C-5)}$$

The resulting coefficient of performance P_c will be given by:

$$P_c = \lambda_c \frac{T_{ev}}{T_{co} - T_{ev}}$$

or

$$P_c = (0.536 - 0.0058\, t_o)\, \frac{(t_i + 0.2\, t_o + 250.0)}{(0.6\, t_o - t_i + 44.55)} \qquad \text{(C-6)}$$

For instance, taking the inside and outside air temperatures of the office building during the cooling mode as t_o = 25.83°C (78.5°F), t_i = 25.55°C (78°F), then t_{ev} = 7.61°C (45.7°F), Δt_{ev} = 17.9°C (32.3°F), Δt_{co} = 16.27°C (29.3°F), t_{co} = 42.1°C (107.8°F), λ_c = 0.5, and the heat pump performance P_c from Eq. C-6 is found to be 3.14. Although heat pumps with different capacity and design features, differ in their performance, the above relationships are considered valuable not only for A-A heat pumps but for any other media in contact with the refrigerant coils.

II. Heating Mode

The new evaporator and condenser temperature levels in the heating mode will be as illustrated in Fig. C-2. The evaporator-side temperature difference Δt_{ev}, could be approximated by:

$$\Delta t_{ev} = t_o - t_{ev} = 9.29 + 0.21\, t_o \qquad \text{(C-7)}$$

hence,

$$t_{ev} = -9.29 + 0.21\, t_o \qquad \text{(C-8)}$$

Also, at the condenser side, the temperature difference Δt_{co} is obtained from:

$$\Delta t_{co} = t_{co} - t_i = 20.24 + 0.67\, t_o \qquad \text{(C-9)}$$

or

$$t_{co} = 20.24 + 0.67\, t_o + t_i \qquad \text{(C-10)}$$

An actual heat pump in the heating mode will be roughly as efficient as a fraction λ_h of the Carnot cycle heat pump operating between T_{ev} and T_{co}. The fraction λ_h is found close to a constant value of 0.45 and the resulting coefficient of performance P_h becomes

$$P_h = \lambda_h \frac{T_{co}}{T_{co} - T_{ev}} \qquad \text{(C-11)}$$

or

$$P_h = 0.45 \frac{(293.4 + 0.67\, t_o + t_i)}{(29.53 + t_i - 0.12\, t_o)} \qquad \text{(C-12)}$$

If, for instance, the space inside and outside temperatures t_i and t_o are 22.22°C (72°F) and 11°C (51.8°F), respectively, they result in a P_h value, using Eq. C-12, of 2.88. Both of the temperature differences Δt_{ev} and Δt_{co} then become 11.6°C (20.9°F) and 27.61°C (49.7°F), respectively. Equations C-6 and C-12 are used to determine monthly P_c and P_h values for each mode of operation as described in the text.

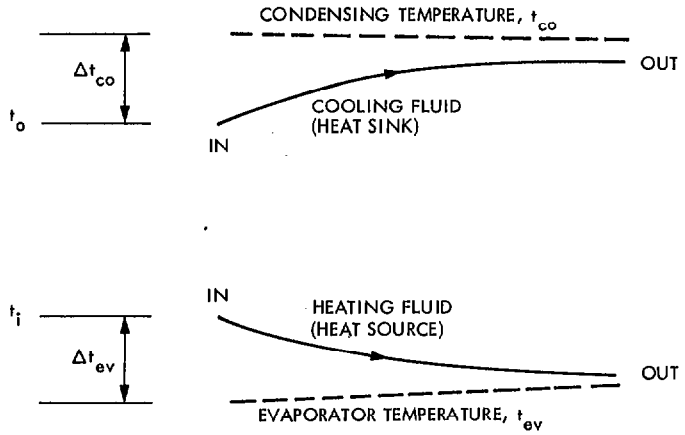

Fig. C-1. Temperature levels of a heat pump in a cooling mode

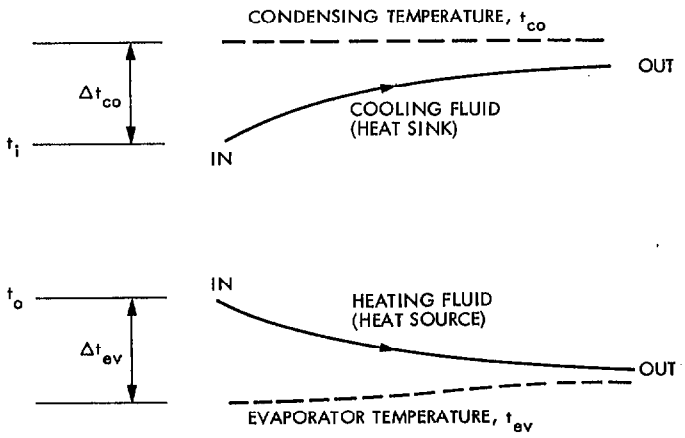

Fig. C-2. Temperature levels of a heat pump in a heating mode